Source apportionment of hydrogen sulphide at Elandsfontein in Mpumalanga Highveld

E Cogho

orcid.org 0000-0001-9748-4184

Dissertation submitted in fulfilment of the requirements for the degree *Master of Science in Environmental Sciences with Atmospheric Chemistry* at the North-West University

Supervisor:	Prof JP Beukes
Co-supervisor:	Prof PG Van Zyl

Graduation July 2019

23474696

Acknowledgments

I would like to thank the following people without whom the completion of my dissertation would not have been possible:

- My supervisors, professors Paul Beukes and Pieter van Zyl, for their guidance, input and support;
- my parents, Viktor and Anneke Cogho, for their belief, support, motivation and love;
- my Father in Heaven, for providing me with the opportunity, perseverance and knowledge.

"Yes, I am the vine, you are the branches. Those who remain in me, and I in them, will produce much fruit. For apart from me you can do nothing." John 15:5

Abstract

As far as the candidate could assess, no H_2S source apportionment has been conducted for the Mpumalanga Highveld, an area with known air quality problems. The lack of such assessments is due to current receptor-oriented methods not being ideal for source apportionment of trace gases and the absence of a comprehensive South African specific emission inventory in the peer reviewed public domain, which is vital for source-oriented models.

In this study, a relatively recently published receptor-oriented source apportionment method, which is applied to conduct equivalent black carbon (eBC) source apportionment, was further developed to enable source apportionment of trace gases. This improved method was successfully applied to conduct H_2S receptor-oriented source apportionment on a data set that was gathered during the European Integrated Project on Cloud Climate, Aerosols and Air Quality (EUCAARI) project at the Elandsfontein measurement station on the Mpumalanga Highveld.

The results proved that urban emissions (associated with towns, as well as semi- and informal settlements, waste water treatment facilities, landfills, small industries and traffic) contributed most to ambient H_2S (41.3% in excess of the baseline), followed by the Johannesburg-Pretoria conurbation (15.3%) and the petrochemical operation near Secunda (14.3%). Pyrometallurgical smelters, coal-fired power stations and cattle feedlots contributed 11.2, 5.9 and 1.0% to ambient H_2S in excess of the baseline, respectively. A total of 89% of the measured ambient H_2S in excess of the baseline was attributed to specific sources, proving that the developed method is an effective tool for source apportionment of trace gases.

Keywords: Receptor-oriented source apportionment, atmospheric trace gases, hydrogen sulphide (H_2S), Mpumalanga Highveld, South Africa

Table of contents

List of abbreviations

ACRG	Atmospheric Chemistry Research Group
ARL	Air Resources Laboratory
CH_4	Methane
CMB	Chemical mass balance
CO	Carbon monoxide
CO_2	Carbon dioxide
DEA	Department of Environmental Affairs
eBC	Equivalent black carbon
EUCAARI	European Integrated Project on Cloud Climate, Aerosols and Air Quality
FA	Factor analysis
GDAS	Global Data Assimilation Service
H_2S	Hydrogen sulphide
H_2SO_4	Sulphuric acid
HNO_3	Nitric acid
HYSPLIT	Hybrid Lagrangian Integrated Trajectory
Jhb-Pta	Johannesburg-Pretoria
MAAP	Multi-angle absorption photometer
NAAQS	National ambient air quality standard
NCEP	National Centre for Environmental Prediction
NH_3	Ammonia
NO	Nitrous oxide
NO_2	Nitrogen dioxide
NO_x	Oxides of nitrogen

NO_3^-	Nitrate
NOAA	National Oceanic and Atmospheric Administration
NWU	North-West University
O_3	Ozone
PC	Principal component analysis
PM	Particulate matter
PMT	Photo multiplier tube
Ppb	Parts per billion
Ppt	Parts per trillion
S^0	Elemental sulphur
SO_2	Sulphur dioxide
SO_4^{2-}	Sulphate
UV	Ultra violet
VOC	Volatile organic compound
USNWS	United States National Weather Service

List of figures

Chapter 2

Chapter 3

Chapter 4

List of tables

Chapter 4

Appendix A

Chapter 1: Background, motivation and objectives

In this chapter, the background information that led to the motivation of this project (Par. 1.1) is briefly considered. Thereafter, in Par. 1.2, the general aim and specific objectives are presented.

1.1 Background and motivation

Although not published, the general opinion of researchers, representatives of the Department of Environmental Affairs (DEA) and the general population is that the petrochemical operation situated near Secunda is the major emitter of hydrogen sulphide (H_2S) in the Mpumalanga Highveld (Cardoso *et al*., 1997; https://cer.org.za/wp-content/uploads/2014/06/2014-06-16-LRC-SASOL-NATREF-postponement.pdf, accessed 30 May 2019). Eskom, for instance, installed an H_2S monitoring instrument at their Elandsfontein atmospheric measurement station (Collet *et al.,* 2010) to capture the influence of the petrochemical operation. However, no H_2S source apportionment studies have thus far been conducted for the Mpumalanga Highveld. The lack of such studies can at least partially be attributed to the fact that almost all receptor source apportionment studies in South Africa have only been undertaken on particulate matter/aerosols (e.g. Maenhaut *et al*., 1996; Engelbrecht *et al*., 2002; Van Zyl *et al*., 2014; Tiitta *et al*., 2014; Venter *et al*., 2017; Jaars *et al*., 2018) or precipitation/deposition (e.g. Mphepya *et al*., 2004 and 2006; Conradie *et al*., 2016), without considering trace gas concentrations.

The Atmospheric Chemistry Research Group (ACRG) at the North-West University (NWU) recently published a paper indicating that concurrently and continuously measured equivalent black carbon (eBC, definition according to Petzold *et al.,* 2013) and trace gas concentrations, considered in context of calculated back trajectories, can be used to identify different sources and to do receptor source apportionment of eBC (Chiloane *et al*., 2017). Although the aforementioned paper focussed on eBC, it was indicated that not all ambient H_2S on the Mpumalanga Highveld can be attributed to the petrochemical operation near Secunda, since H_2S associated with eBC was used to identify emissions from the pyrometallurgical smelters in the Witbank and Middelburg area (Chiloane *et al*., 2017). This does not imply that the petrochemical operation does not emit H_2S, but it certainly proves that it is not the only emitter in the area.

Currently there is no South African national ambient air quality standard (NAAQS) for H_2S (DEA, 2009). However, the DEA stipulates that if any hourly average concentration of H_2S exceeds 29 ppb in a day, that day is regarded as a high H_2S day (DEA, 2009). In order for the DEA to regulate ambient H_2S levels and/or emission sources meaningfully, source apportionment studies are required. Considering the aforementioned context, the source apportionment technique developed by the ACRG (Chiloane et al., 2017) was developed further in this study to enable receptor source apportionment studies of

trace gases, including H_2S at Elandsfontein. The Elandsfontein site was chosen as it is situated within the Mpumalanga Highveld, central to multiple different point sources. However, not close enough to any of the sources to create a bias to a specific source. Additionally, a comprehensive dataset was acquired at Elandsfontein during the EUCAARI project (Laakso *et al*., 2012).

1.2 Objectives

The general aim of this study was to do source apportionment of H_2S at Elandsfontein in the Mpumalanga Highveld. To reach this aim, the following specific objectives needed to be reached:

I.) Modify and further develop the existing source apportionment method presented by Chiloane *et al.* (2017) to enable source apportionment of trace gases.

II.) Identify unique characteristics, e.g. coincidental concentration peaks, plume times, duration and amplitude, and air mass movements, to isolate different H_2S sources.

III.) Conduct a source apportionment study of H_2S measured at Elandsfontein.

Chapter 2: Literature survey

In this chapter, the literature survey for this study is presented. Par. 2.1 starts with a general discussion of atmospheric pollutants, which leads to Par. 2.2, wherein hydrogen sulphide (H_2S), i.e. the pollutant of interest in this study, is considered in more detail. Source apportionment of atmospheric pollutants, the different techniques applied in source apportionment methods and the shortcomings thereof are discussed in Par. 2.3. The chapter closes with Par. 2.4, which presents conclusions from literature.

2.1 Atmospheric pollutants

Due to many different sources and possible transformations of emitted species, a multitude of different pollutants occur in the atmosphere. Atmospheric pollutants can broadly be divided into two categories, i.e. i) gases and ii) aerosols/particulate matter (PM). Furthermore, both gaseous and aerosol/PM species can be divided into primary and secondary pollutants. Primary pollutants are emitted directly into the atmosphere and secondary pollutants occur because of physical and chemical transformations of primary pollutants during transportation/ageing.

2.1.1 Gaseous pollutants

Gaseous pollutants can be organic or inorganic in nature (Kampa & Castanas, 2008). Examples of organic species are methane (CH_4), volatile organic compounds (VOCs) and halogenated organic compounds (Daly & Zannetti, 2007; Kampa & Castanas, 2008). Inorganic species include sulphur dioxide (SO_2), hydrogen sulphide (H_2S), ozone (O_3), nitrogen oxide (NO), nitrogen dioxide (NO_2) and carbon monoxide (CO) (Kampa & Castanas, 2008). Many of these pollutants are primary pollutants that are emitted directly into the atmosphere, but they also undergo intrinsic reactions to form secondary pollutants. VOCs play a significant role in new particle formation (Reisell *et al*., 2003) and take part in photochemical reactions with oxides of nitrogen (NO_x) to form O_3 (Atkinson *et al*., 2000; Seinfeld & Pandis, 2006). Some of the primary pollutants can also occur as secondary pollutants, e.g. SO_2 formed from the oxidation of H_2S, CO_2 (carbon dioxide) by oxidation of CO, and less volatile VOCs from more volatile VOCs (Seinfeld & Pandis, 2006).

2.1.2 Aerosols

Aerosols are very small solid or liquid particles suspended in the air, which can differ in shape, morphology, number and size (Kampa & Castanas, 2008). Aerosols are also referred to as particulate matter (PM). Primary aerosols/PM are emitted by numerous anthropogenic (e.g. household combustion, industries, mining operations, farming) and natural (e.g. sea spray, dust storms, volcanic activity) sources (Jayaratne & Verma, 2001; Ross *et al.,* 2003; Vakkari *et al.,* 2011; Laakso *et al.,* 2012). It is also common that primary pollutants reacting in the atmosphere form secondary aerosols such as

organic aerosols formed from gas-to-particulate reactions of VOCs, sulphuric acid (H_2SO_4) from SO_2, and the formation of nitrates (NO_3^-) and sulphates (SO_4^{2-}) from H_2SO_4 and nitric acid (HNO_3) reacting with ammonia (NH_3) (Seinfeld & Pandis, 2006).

2.1.3 Atmospheric pollution in the Mpumalanga Highveld

The highly industrialised South African Highveld is one of the most polluted regions in South Africa, which has one of the largest industrialised economies in the Southern Hemisphere (Freiman *et al.*, 2002; DEA, 2010). Due to regular exceedances of air quality standard limits of criteria pollutants, the area was declared a priority area, i.e. the Highveld Priority Area (HPA), in terms of air quality by the South African government (DEA, 2007). The geographical extent of the HPA includes the Mpumalanga Highveld and a part of the Gauteng province (DEA, 2007), as indicated in Figure 2.1. Various anthropogenic and natural activities in this area contribute to the elevated level of gaseous and aerosol pollutants (DEA, 2010; Lourens *et al.*, 2011).

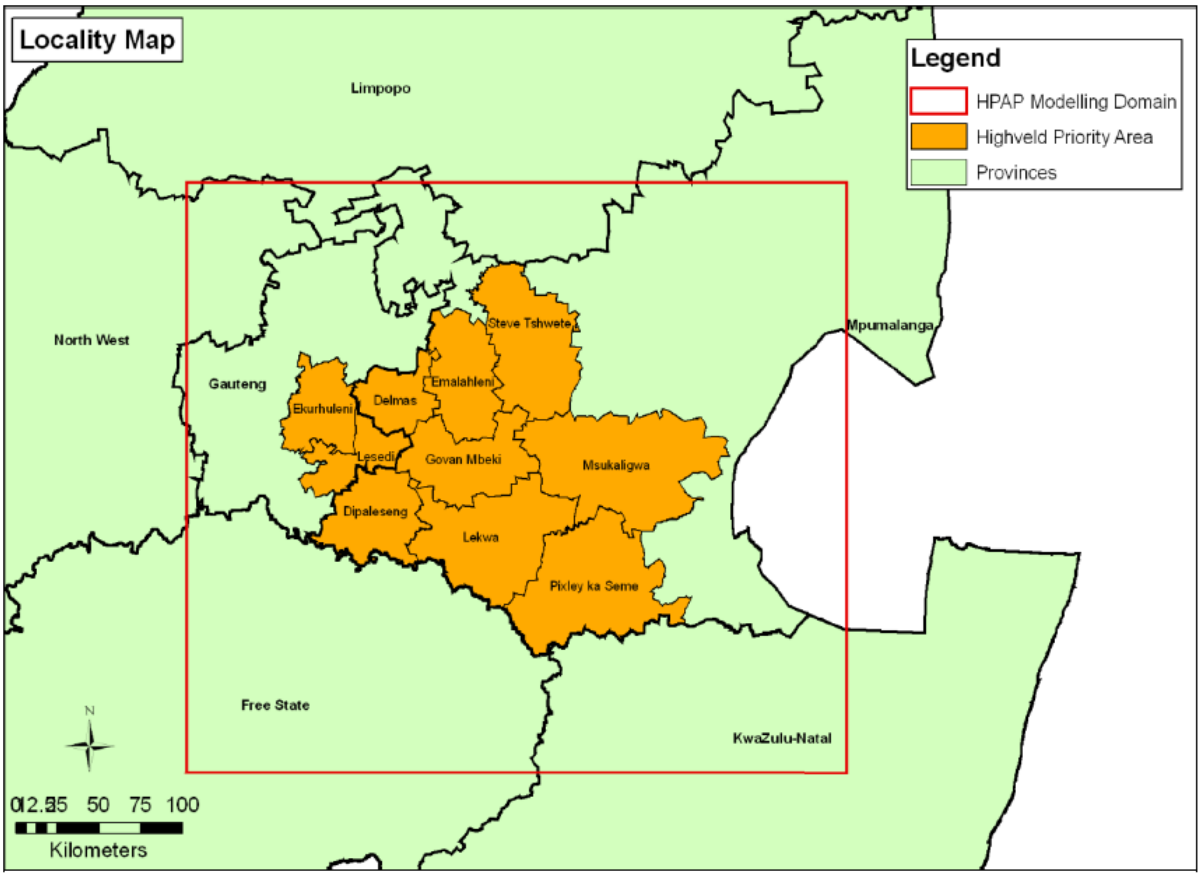

Figure 2.1: Map depicting the geographical extent of the Highveld Priority Area in orange (with permission, DEA, 2010).

Unique meteorological conditions characterise the South African Highveld, with large-scale anti-cyclonic recirculation (Garstang *et al.*, 1996; Tyson *et al.*, 1998), as well as a strongly layered

troposphere with the formation of multiple inversion layers that prevent mixing of the atmosphere at certain times (Garstang *et al*., 1996; Korhonen *et al*., 2014; Gierens *et al*., 2018).

The HPA is home to various anthropogenic sources (Figure 2.1) such as metallurgical smelters, coal-fired power stations, mining industry, petrochemical industry, agriculture and transportation (Fenger, 2009; Dabrowski *et al*., 2008; Freiman *et al*., 2002; DEA, 2010). The cold weather in winter (Jun - Aug) results in additional burning of coal and wood for domestic heating purposes (Novelli, 2003; Laakso *et al*., 2008; Venter *et al*., 2012; Nkosi *et al*., 2018) and the dry climate in May to middle October results in increased anthropogenic open biomass burning (grassland and savannah fires) on the Highveld (Swap *et al*., 2003; Lourens *et al*., 2011; Jayarante & Verma, 2001; Maenhaut *et al*., 1996). The Johannesburg-Pretoria (Jhb-Pta) megacity (Lourens *et al*., 2011 and 2016) is also located to the west of the Mpumalanga Highveld and it further contributes to pollutant concentrations in the area. Figure 2.2 indicates the location of several of the aforementioned anthropogenic atmospheric pollutions sources in, or near the HPA.

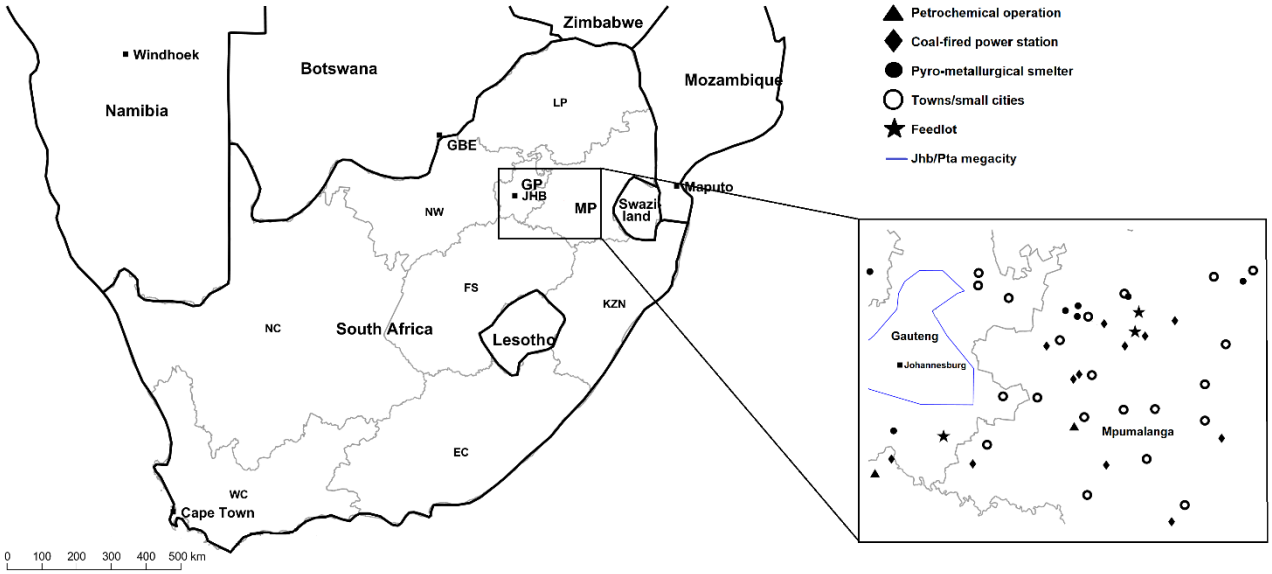

Figure 2.2: Map indicating the location of various anthropogenic point sources in the HPA and surrounding areas, as well as the outline of the Jhb-Pta megacity (blue polygon).

In addition to the abovementioned anthropogenic sources, there are also numerous natural sources of atmospheric pollutants that influence the HPA, e.g. biogenic emissions, soil surfaces, the Indian ocean and other aqueous surfaces, dust storms, and decompositions of animal and plant material (Jaars *et al*., 2016; Williams & Baltensperger, 2009).

Regular exceedances of NAAQS limits have been (and still are) recorded in the HPA. For instance, in the HPA air quality baseline assessment report the following exceedances were reported over a three-year period (2004-2006): NO_2 exceeded its 1 hour standard of 106 ppb 119 times, O_3 exceeded its 8

hour standard of 61 ppb 426 times, the 24 hour PM_{10} standard of 120 ug/m^3 was exceeded 182 times and the 24 hour and 1 hour standards for SO_2 of 48 ppb and 134 ppb were exceeded 86 and 762 times, respectively over the three years (DEA, 2010). The HPA is also considered as one of the major NO_2 hotspots in the world (Wenig *et al*., 2003; Lourens *et al*., 2012) and it was previously estimated that 91% of the NO_x emissions in South Africa are from the Mpumalanga province (Wells *et al*., 1996).

2.2 H_2S

Although many criteria and non-criteria pollutants are problematic in the HPA, H_2S was chosen as the atmospheric pollutant of interest, as motivated in Chapter 1. H_2S is a flammable, colourless gas with a distinct odour of rotten eggs at very low concentrations. The human detection threshold of H_2S is approximately 0.48 ppb (WHO, 2003) – this is the concentration at which 50% of the human population can detect H_2S gas. H_2S has negative human and environmental impacts. Short-term exposure to high (e.g. > 10 000 ppb) H_2S concentrations can cause health effects, including respiratory, ocular, neurological, cardiovascular, metabolic and reproductive effects and in extreme cases of exposure could result in fatalities (Rayner-Canham & Overton, 2009; WHO, 2003). H_2S is also considered to be more toxic than hydrogen cyanide (Rayner-Canham & Overton, 2009). Notwithstanding the aforementioned, there is currently no South African national ambient air quality standard (NAAQS) for H_2S (DEA, 2010).

H_2S is a key compound in the global sulphur cycle, of which a simplified flow chart is depicted in Figure 2.3. The anaerobic breakdown of sulphur by sulphur-reducing bacteria produces H_2S in the environment (Reaction 2.1) and this process is the source of most of the naturally occurring sulphur in the atmosphere. Approximately 90% of H_2S emitted is of natural origin through the anaerobic break down of sulphur containing material and other natural sources (e.g. volcanic gases, sulphur deposits and sulphur springs) (EPA, 1993).

$$H_2SO_4 + 2CH_2O \rightarrow 2CO_2 + 2H_2O + H_2S \quad (2.1)$$

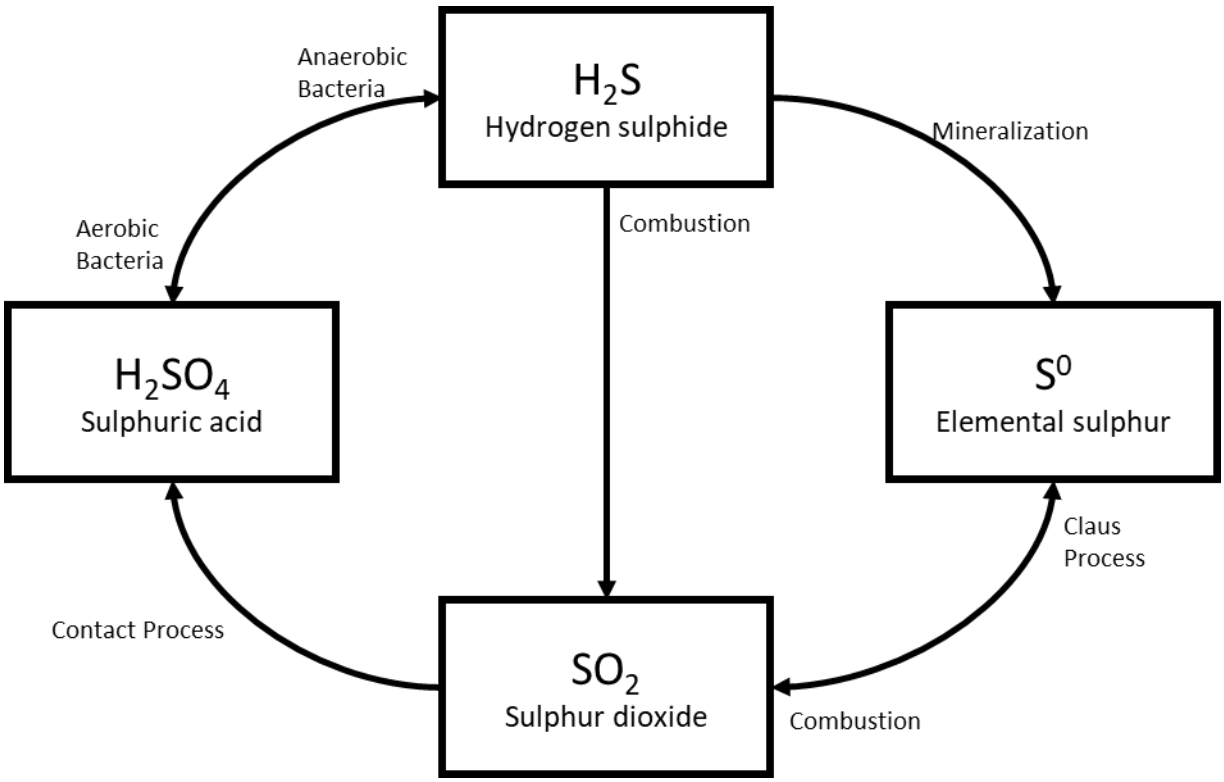

Figure 2.3: The participation of H_2S in the global sulphur cycle (Rubright et al., 2017).

Anthropogenic H_2S emissions occur by way of a variety of industrial processes (Rayner-Canham & Overton, 2009; Camacho, 2009; Rubright *et al.,* 2017) such as in the petrochemical (extraction and refining of natural gas and oil) and pyrometallurgical industries (if a reducing environment is present), and from the paper manufacturing industry. Other anthropogenic sources include sewage plants, tanneries, pyrometallurgical coke oven plants and manure-handling facilities (Chou *et al*., 2016).

Furthermore, H_2S undergoes numerous intrinsic reactions to produce different sulphur-containing compounds such as sulphuric acid (H_2SO_4), elemental sulphur (S^0) and SO_2. A typical reaction of this kind is anoxygenic photosynthesis, where bacteria uses light energy as energy source for the bonding of inorganic carbons onto organic materials, with H_2S acting as an electron donor to produce S^0 and H_2SO_4 (Camacho, 2009). Reactions 2.2 and 2.3 depict how H_2SO_4 and S^0 are formed in this manner.

$$2H_2S + CO_2 \rightarrow CH_2O + H_2O + 2S^0 \quad (2.2)$$

$$H_2S + 2CO_2 + 2H_2O \rightarrow 2CH_2O + H_2SO_4 \quad (2.3)$$

Chemotrophic sulphur oxidation is yet another bacterial reaction where prokaryotes (uni- or multicellular organisms that lack a membrane-bound nucleus or mitochondria) use H_2S as an energy

source for their metabolism. A characteristic reaction used by these chemolithotrophic bacteria is the aerobic oxidation of H_2S with oxygen (O_2), as seen in Reaction 2.4 (Camacho, 2009).

$$H_2S + ½O_2 \rightarrow S^0 + H_2O \quad (2.4)$$

In the atmosphere, H_2S acts as a precursor for SO_2 when it reacts with the hydroxyl radical ($OH^\bullet$) to form an $HS^\bullet$-radical, whereafter the radical undergoes numerous reactions to form SO_2 (Seinfield & Pandis, 2006; Rubright *et al.,* 2017):

$$H_2S + OH^\bullet \rightarrow HS^\bullet + H_2O \quad (2.5)$$

$$HS^\bullet + O_2 \rightarrow HO^\bullet + SO \quad (2.6)$$

$$SO + O_2 \rightarrow SO_2 + O \quad (2.7)$$

Atmospheric ozonation of H_2S (the oxidation of H_2S with O_3) can also occur to produce SO_2 (Hales *et al.,* 1973):

$$H_2S + O_3 \rightarrow SO_2 + H_2O \quad (2.8)$$

H_2S undergoes combustion reactions in air to produce SO_2 (Reaction 2.9) or elemental sulphur (Reaction 2.10) (Rayner-Canham & Overton, 2009; Rubright *et al.,* 2017):

$$2H_2S + 3O_2 \rightarrow 2H_2O + 2SO_2 \quad (2.9)$$

$$2H_2S + O_2 \rightarrow 2H_2O + 2S \quad (2.10)$$

In industrial processes, H_2S is converted to elemental sulphur by way of the Claus process to limit H_2S emissions. First the H_2S is burned with oxygen present to produce SO_2 (Reaction 2.11), with the remaining H_2S then reacted with SO_2 to produce elemental sulphur (Reaction 2.12) (Goar *et al.,* 1986; Scott, 1992).

$$2H_2S + 3O_2 \rightarrow 2SO_2 + 2H_2O + \text{heat} \quad (2.11)$$

$$2H_2S + SO_2 \rightarrow 3S + 2H_2O + \text{heat} \quad (2.12)$$

The Claus process is not 100% effective in removing H_2S gas from off-gas emissions (Goar *et al.,* 1986; Scott 1992). Thus, even if industries use the Claus process to eliminate H_2S emissions, a small fraction of the produced H_2S will still be emitted. As an example, it has been reported that the petrochemical operation near Secunda in the HPA does have methods in place to remove H_2S from the off-gas, but, according to an atmospheric impact report, a fraction of H_2S is still emitted (Airshed Planning Professionals, 2017).

2.3 Source Apportionment

To design and implement air quality policies it is essential to have information on pollution sources (Belis *et al*., 2014). Thus, identifying the different sources of atmospheric pollutants and quantifying their contribution to ambient air pollution, i.e. source apportionment (Belis *et al*., 2014), is an important information gathering process. Mainly two different approaches to conduct source apportionment are currently applied, i.e. i) source-oriented models and ii) receptor-oriented models (Belis *et al*., 2014; Viana *et al*., 2008). In Figure 2.4, a schematic representation of these two approaches is presented, as well as some common techniques used within these methods to conduct source apportionment. These two approaches and their associated techniques will be discussed in more detail in the following two paragraphs.

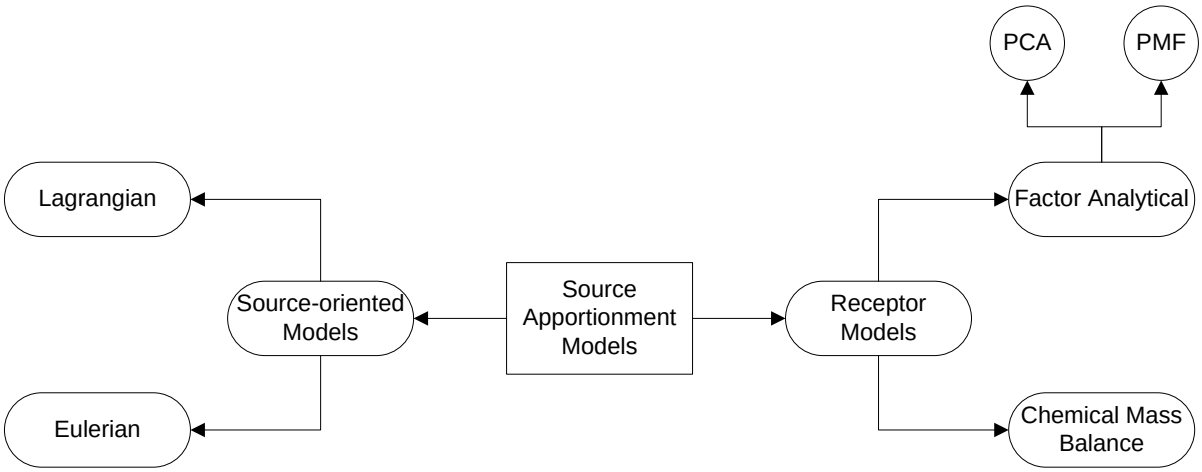

Figure 2.4: Schematic representation of the two main approaches used to conduct source apportionment and the common techniques used therein.

2.3.1 Source-oriented models

Source-oriented techniques do source apportionment by using emission inventories to simulate the processes of emission, transport, physical and chemical alterations, and the deposition of atmospheric pollutants (Doraiswamy *et al*., 1995; Eldering & Cass, 1996; Visser *et al*., 2001; Viana *et al*., 2008). However, these techniques are highly reliant on accurate emission inventories – databases that indicate the amount of pollutants emitted into the atmosphere per time unit at either the discrete location of sources, or sources allocated within grid cells, to get the correct spatial coverage (EPA, 2018). However, using these models has been challenging, as there are no comprehensive peer-reviewed inventories available in the public domain for South Africa. According to South African environmental legislation, significant emitters have to supply atmospheric emission data to government. However, this data is supplied with some legal safeguards, which have thus far prevented a comprehensive peer-reviewed emission inventory becoming available in the public domain. Interested and affected parties can use the Promotion of Access to Information Act 2 of 2000 (PAIA)

(http://www.dirco.gov.za/department/paia.pdf, accessed 4 March 2019) to attempt to obtain such information, but this process is lengthy and costly, and does not always yield all the required information. In addition, emissions from area sources of which the spatial coverage and emission factors do not stay constant (e.g. open biomass burning), and sources such as household combustion in semi- and informal settlements that are difficult to regulate complicate the South African situation further. Therefore, the vast majority of source-oriented atmospheric modelling studies undertaken for this region have used global emission inventory databases (e.g. Tummon *et al*., 2010; Laakso *et al*., 2013; Kuik et al., 2015; Lourens et al., 2016), which do not always contain enough detailed information. Typical source-oriented methods apply the a) Eulerian and b) Lagrangian techniques.

a) Lagrangian techniques

In these models, a moving framework of reference is used to describe the trajectories of, for instance, particles or aerosols as they move through the atmosphere. This can be done for single- or multiple particles (Belis *et al.,* 2014). For example, Bhave *et al*. (2001) used a source-oriented Lagrangian trajectory model to generate synthetic data sets of source-segregated single particles, with the model including aerosol processes such as emission, transportation, deposition, gas-phase transformations and fog chemistry (Bhave *et al.,* 2001).

Various South African source-oriented studies have used Lagrangian models. For instance, a Lagrangian kinematic model was used by Freiman & Piketh (2002) to model air transport in the industrial Highveld of South Africa. It was discovered that 43% of air reaching the Highveld was clean marine air and that 25% of all air transported to the Highveld region is loaded with aerosols from subtropical Africa (Freiman & Piketh, 2002). Bruwer & Kornelius (2017) used a CALPUFF dispersion model to simulate the deposition rates for nitrogen- and sulphur-containing species. To determine the impact of biogenic emissions of NO_x on the Highveld, the model was applied with and without biogenic emissions of NO_x (Bruwer & Kornelius, 2017). The results indicated that biogenic NO_x emitted in the Highveld contributed significantly more than emissions from household combustion, open biomass burning and small industries (Bruwer & Kornelius, 2017).

b) Eulerian techniques

Eulerian models incorporate chemical and physical (motion and other physical processes/transformations) equations that are solved at selected points on a three-dimensional grid (Belis *et al.,* 2014). These models are better suited for secondary pollutants, as they account for the chemical interactions between sources (Yarwood *et al.,* 2007). As an example, Kleeman (2001) developed a three-dimensional source-oriented model for externally mixed aerosols to conduct source apportionment in the South Coast Air Basin surrounding Los Angeles. The model

simultaneously tracked fine/inhalable particle concentrations, ozone and other gaseous species (Kleeman *et al.,* 2001).

Transport and the deposition of sulphur over South Africa was modelled by Zunckel *et al*. (2000) with the MATCH Eulerian model. Modelled wet deposition rates of sulphur for the Highveld was between 1 and 5 kg S ha^{-1} a^{-1} (Zunckel *et al*., 2000). Laakso *et al*. (2013) used the GLOMAP model, which is an extension of the TOMCAT 3-D Eulerian model, to simulate particle growth in South Africa. However, they found that the model did not reproduce the particle growth characteristics of observations (Laakso *et al*., 2013).

2.3.2 Receptor models

Receptor models apply multivariate statistical techniques to identify and quantify air pollutants to their sources (Hopke, 2008; 2011 and 2016). These models are based on the fundamental principle that mass conservation takes place between the emission site and receptor site. A mass balance analysis is used by most receptor modelling techniques for the identification and apportionment of PM/aerosols (Cooper & Watson, 1980; Hopke, 2008; 2011 and 2016). An equation is written to account for all *m* chemical species in the *n* samples as contributions from *p* independent sources (mass balance equation, Equation 2.1).

$$x_{ij} = \sum_{p=0}^{p} g_{ip} f_{pj} + e_{ij} \quad (2.1)$$

with x_{ij} equal to the measured concentration of the j_{th} species in the i_{th} sample, f_{pj} is the concentration of the j_{th} species in material emitted by source p, g_{ip} is the contribution of the p_{th} source to the i_{th} sample and e_{ij} is the portion of the measurement that cannot be fitted by the model.

Naturally, any model developed for the identification and apportionment of atmospheric pollutants will have some physical constraints (Henry, 1991). It is therefore important to consider these limitations/difficulties before developing any model. For receptor modelling, the fundamental constraints that need to be adhered to are (Hopke *et al.,* 2008):

- The model must reproduce the original data and explain the observations;
- non-negative source compositions must be predicted, a negative concentration cannot be obtained by a source;
- the sum of the predicted source contributions must be less or equal to the total measured mass/concentrations of each element.

Typical receptor models are a) chemical mass balance models(CMB) and b) factor analytical (FA) methods such as i) principle component analysis (PCA) and ii) positive matrix factorisation (PMF), with all of these methods taking different routes to solve the mass balance equation (Equation 2.1).

a) Chemical mass balance

In CMB models, the sources of pollutants must be known to conduct the analysis (Hopke *et al.,* 2008). These models solve the mass balance equation (Equation 2.1) by using effective variance least squares. To solve this equation, the number (p) and composition of sources (f_{pj}) must be known, which leaves only the contribution (g_{ip}) as unknown (Hopke *et al.,* 2008; Belis *et al.,* 2014). CMB software can be readily obtained from the U.S. EPA (Environmental Protection Agency) at www.epa.gov/SCRAM. Although CMB is an effective receptor modelling technique for primary PM, it is not able to effectively deal with secondary PM (Hopke *et al.,* 2008).

CMB source apportionment has been applied within the South African context. For instance, in a study by Maenhaut *et al*. (1996), CMB was done after PCA was first applied to identify the possible sources – as previously stated, CMB is more appropriate if the major sources are already known (Maenhaut *et al*., 1996). It was discovered that, in the Highveld, mineral dust and sea salt contributed in a ratio of 99 to 1 to the course PM fraction and the pyrogenic component was the dominant contributor in the fine PM fraction (Maenhaut *et al*., 1996). Engelbrecht *et al*. (2002) used a CMB model to compare source contributions from residential coal and low-smoke fuels in the Qalabotjha township. The study confirmed that the greatest source of PM in the township was residential combustion of coal, followed by biomass burning (Engelbrecht *et al*., 2002).

b) Factor analytical techniques

FA methods (e.g. PCA and PMF) are multivariate techniques that aim to solve the mass balance equation (Equation 2.1). These methods do not require information about the number and composition of the sources under investigation for input (Hopke *et al.,* 2008; Belis *et al.,* 2014). However, detailed source knowledge is required from the user to relate modelled source profiles to specific sources (Viana *et al*., 2008). These methods gain information on source contributions by the variability of different elements in large data sets (Cooper, 1980; Hopke *et al.,* 2008). It has been suggested that factor analytical methods tend to retrieve more information from atmospheric data than there actually is (Henry, 1987). Regardless of this, these methods are often used for source apportionment, as software packages to do the studies are widely available and no prior information of sources and emission profiles are required (Viana *et al.,* 2008).

i) Principal component analysis

PCA is a multivariate data analytical technique used to correlate a large number of variables into a smaller number of variables known as principle components (Wold *et al.,* 1987; Adbi & Williams, 2010). The principle components are uncorrelated with each other and orthogonal (Pires *et al.,* 2007). The components are linear combinations of the original variables in a way that the first component

represents the largest portion of the data variability, the second component represents a lesser portion than the first and so forth (Abdul-Wahab *et al.,* 2005; Sousa *et al.,* 2007; Wang & Xiao, 2004). The influence of each original variable on the different components are determined by running a rotational algorithm (e.g. Varimax rotation), which calculates the rotated factor loadings and represents each variable's contribution to the principle components (Pires *et al.,* 2007). Pires *et al.* (2007; 2008), for example, used PCA to classify atmospheric monitoring sites and sort them into classes according to their pollution behaviours in terms of SO_2 and PM, as well as NO_2, CO and O_3.

As previously stated, Maenhaut *et al*. (1996) used PCA to first determine the main sources (components) of aerosols before applying CMB. Components for the course PM fraction were mineral dust and sea salt, while four components were identified in the fine fraction, i.e. sea salt, sulphate, mineral dust and biomass burning (Maenhaut *et al*., 1996). Conradie *et al*. (2016) used PCA as an exploratory tool to determine sources influencing wet deposition at four sites in South Africa, i.e. Amersfoort, Vaal Triangle, Louis Trichardt and Skukuza. For Amersfoort crustal, combustion of fossil fuel and marine- and agricultural components were identified as possible sources (Conradie *et al*., 2016). Identifying sources in the Vaal Triangle proved more difficult since it is a complex site surrounded by numerous industries and anthropogenic sources. The sources for Skukuza and Louis Trichardt were divided into two components: i) species associated with crustal and marine sources and ii) species associated with agricultural- and fossil fuel combustion sources (Conradie et al., 2016).

ii) Positive matrix factorisation

PMF is a specific type of factor analytical method that uses the experimental uncertainty for scaling matrix elements and coerces factor elements to be non-negative (Belis *et al.,* 2014). The most significant problem in PMF is to determine the identity and contribution of different components in an unfamiliar mixture (Malinowski *et al.,* 2002; Reff, 2007). The most common PMF model is a bilinear model where observations of PM species are expressed as the sum of contributions from several different time-invariant source profiles (Reff, 2007). The model deconstructs the data into two matrices, i.e. factor profiles and factor contributions, with the aim to classify the specified quantity of factors, which are viewed as sources (Jaars *et al.,* 2018). Contini *et al*. (2016) used PMF to determine the contribution of a large coal-fired power station to PM_{10} concentrations in Italy. The contributions of the power station were approximately 2% of primary PM in the study area (Contini *et al*., 2016).

Recently, Jaars *et al*. (2018) used PMF to conduct a source apportionment study on VOCs measured at a regional background site in the interior of South Africa. They differentiated ten meaningful factors for VOCs. Five of these factors were associated with biogenic emissions and the other five were from anthropogenic sources (Jaars *et al*., 2018). From the biogenic factors, three factors could be

characterised by specific species (i.e. limonene, isoprene and 2-methyl-3-buten-2-ol) and the other factors were made up of biogenic mixtures and tracer species (Jaars *et al*., 2017).

2.4 Conclusion from literature survey

H_2S is a toxic atmospheric pollutant that can affect the respiratory-, ocular-, neurological-, cardiovascular-, metabolic- and reproductive systems in the human body. Severe cases of H_2S exposure may result in death. Considering the pungent odour, detrimental effects and atmospheric chemistry of H_2S, national and/or regional specific (e.g. for the HPA) South African ambient air quality standards are likely to be considered in future. To do so, knowledge of the emissions and background concentration of H_2S is needed. The general belief of the scientific- and governmental communities at present is that H_2S is mainly emitted by the petrochemical operation near Secunda (Cardoso *et al*., 1997; https://cer.org.za/wp-content/uploads/2014/06/2014-06-16-LRC-SASOL-NATREF-postponement.pdf, accessed 30 May 2019). However, no source apportionment studies to prove this have been done. Numerous anthropogenic and natural sources of H_2S are situated in the HPA.

From the literature survey, it is evident that there are gaps/shortcomings in atmospheric pollutant source apportionment studies for South Africa. These include the need for South African specific emission inventories for source-oriented models and receptor modelling studies that focus only on PM/aerosols without considering trace gasses.

Considering the shortcomings in source apportionment techniques, the severity of trace gas pollution in the HPA, and specifically the lack of knowledge on H_2S pollution, it is of outmost importance to conduct a source apportionment study on H_2S for the HPA. The literature survey therefore supports the objectives set in Par. 1.2. To reach these objectives, a novel receptor-oriented source apportionment method, recently presented by Chiloane *et al*. (2017), was improved and applied.

Chapter 3: Methodology

In this chapter, information regarding the methodologies used is presented. Firstly, in Par. 3.1, the site description for the Elandsfontein atmospheric measurement station, where the ambient atmospheric pollutant concentration data used in this study were collected, is presented. The instrumentation used for atmospheric measurements and ancillary data are then considered in Par. 3.2, while data cleaning and quality control/assurance are discussed in Par. 3.3.

3.1 Site description

The measurement data set gathered at the Elandsfontein measurement station during the South African portion of the European Integrated Project on Cloud Climate, Aerosols and Air Quality (EUCAARI) project (Laakso *et al*., 2012) was used during this study (2009-2011). Elandsfontein, which is an ESKOM operated measurement site, lies on a hilltop approximately 200 km east of Johannesburg (Collet *et al.,* 2010) and the position thereof (26° 14'43 S, 29° 25'30 E, 1750m above sea level) within a regional context is indicated by the red star in Figure 3.1.

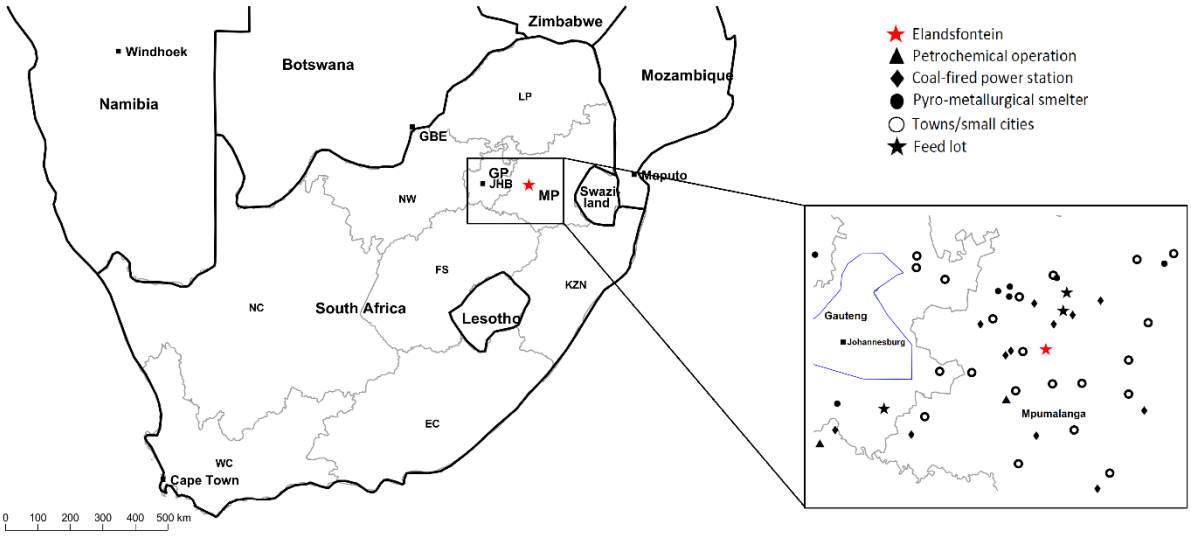

Figure 3.1: Map indicating the position of the Elandsfontein measurement site in South Africa, as well as the position of the site relative to potential anthropogenic atmospheric sources in the area. The blue polygon in the zoomed-in map section indicates the Johannesburg-Pretoria megacity.

The immediate surroundings of the site are mainly grassland (Mucina & Rutherford, 2006) and cultivated land, as seen in the Google Earth Image in Figure 3.2. No large point sources occur within an approximate 15 km radius of the station.

Figure 3.2: Google Earth image of the Elandsfontein measurement station and the immediate surrounding environment. In the image the red line indicates a ruler of 100m (for scaling purposes).

Within a 100 km radius of the station, numerous pyrometallurgical smelters, several coal-fired power stations and a large petrochemical operation can be found (Laakso *et al.,* 2012). In addition to the large point sources in the area, there are also multiple area sources such as towns, landfills, burning coal dumps, cattle feedlots, traffic, open biomass burning, domestic fuel burning, waste burning, as well as marshlands and still standing water reservoirs. Another large area source relatively close by is the Johannesburg-Pretoria (Jhb-Pta) megacity/conurbation, which is a large pollution source in the South African Highveld (Lourens *et al*., 2012 and 2016). The Jhb-Pta megacity is depicted with a blue polygon in Figure 3.1. From the aforementioned descriptions it is evident that the study area has a high density and variety of air pollution sources, thus making it a complex area for air quality studies, especially for the source apportionment of gas species.

3.2 Instrumentation

A comprehensive set of instruments were deployed during the EUCAARI measurement period at Elandsfontein. This included measurements of new particle formation and subsequent particle growth with a Scanning Mobility Particle Sizer (SMPS); aerosol optical properties with a Multi-Angle Absorption Photometer (MAAP), a 3-wavelength Particle Soot Absorption Photometer (PSAP) and an Ecotech Aurora 3000 3-wavelength nephelometer; solar irradiance and aerosol optical depth with a Cimel multichannel Sun photometer; dichotomous aerosol sampler (2025 Partisol) equipped with a PM_{10} inlet and cyclone splitter for collection of filter-based particulate matter (PM) with aerodynamic

diameter less than 2.5 µm ($PM_{2.5}$) and aerodynamic diameter between 2.5 and 10 µm ($PM_{2.5-10}$) that was analysed off-line for water soluble ions, as well as organic and elemental carbon; and vertical aerosol back scattering profiles with a Raman LIDAR system extended PollyXT. Detailed descriptions of the aforementioned measurements at Elandsfontein and associated results have been published (e.g. Laakso *et al.*, 2012; Backman *et al*., 2014; Korhonen *et al*., 2014; Giannakaki *et al*., 2015; Baars *et al*., 2016), or are currently being considered in other studies (e.g. Venter *et al*., 2019; Sehloho *et al*., 2019). However, such measurements were not considered in this study and are therefore not discussed further.

3.2.1 Trace gas and eBC measurements

Similar to Chiloane *et al.* (2017), simultaneous trace gas and eBC measurements were considered to identify coincidental peaks during the receptor-oriented model applied during this study. Therefore, these measurements are considered in greater detail. Nitrogen oxides (NOx), SO_2, H_2S and eBC were measured using a Thermo Electron 42i NOx analyser (a), a Thermo Electron 43C SO_2 analyser (b), a Thermo Electron 43A with a Thermo Electron 340 converter (c), and Thermo Scientific model 5012 MAAP (d), respectively.

a) NO_x

The Thermo Electron 42i NOx analyser operation is based on the principle that NO reacts with O_3 to produce characteristic luminescence that is linearly proportional to the concentration of NO present. Infrared light is emitted when NO_2 molecules decay to lower energy levels or states (Thermo Fischer Scientific, 2007), more specifically:

$$NO + O_3 \rightarrow NO_2 + O_2 + h\nu \quad (3.1)$$

For NO_2 to be measured, it must first be converted to NO by a molybdenum NO_2-to-NO converter heated to 325°C, to then be measured by the chemiluminescence reaction (Thermo Fischer Scientific, 2007). This results in a total NO_x concentration, from which the initial NO concentration can then be subtracted to calculate the NO_2 concentration.

b) SO_2

The Thermo Electron 43C SO_2 analyser operation is based on measuring the emitted fluorescence of SO_2 that is produced during absorption of ultraviolet (UV) light (EPA, 2009). UV light between wavelengths 190 and 230 nm is focused through the fluorescent chamber. SO_2 absorbs light in this wavelength range and becomes electronically excited. It then emits unique decay radiation, which is measured with a photo multiplier tube (PMT). Light energy impinging on the PMT is converted to a voltage, which is then directly analysed (EPA, 2009).

c) H_2S

H_2S was converted to SO_2 by the Thermo Electron 340 converter and then analysed by the Thermo Electron 43A SO_2 analyser. This analyser operates in the same manner as the Thermo Electron 43C SO_2 analyser by measuring the decay radiation after the absorption of UV light by SO_2, resulting in a total sulphur measurement (EPA, 2009). By bypassing the converter, the analyser measures only non-converted SO_2 and not the SO_2 converted from H_2S. The H_2S concentration is calculated by subtracting the latter from the total sulphur concentration.

d) eBC

The eBC was measured with a Thermo Scientific model 5012 multi-angle absorption photometer (MAAP), for which eBC concentrations were corrected according to an algorithm presented by Hyvärinen *et al.* (2013). The MAAP measures the absorption of light and then uses the mass absorption efficiency of 6.6 m^2g^{-1} to compute eBC concentrations (Laakso *et al.,* 2012). Sample air is drawn in through an inlet and deposits particles on glass-fibre filter tape. Particles collect on the tape where a 670 nm light source is aimed at the deposited particles. Photo detectors measure both the reflected and transmitted light. Thereafter, real time data is calculated by constant integration of the decrease of light transmission, numerous reflection intensities and air sample volume over time (Thermo Fischer Scientific, 2007).

3.2.2 Ancillary measurements

Meteorological parameters were measured with a Vaisala WXT510 meteorological station (Vaisala 2010) that was fitted on the roof of the measurement station building, approximately 3.5 m above ground level. These measurements included wind speed and -direction, temperature, rain intensity and relative humidity. A PAR sensor measured solar radiation and the potential temperature gradient was measured with two Rotonic T-RH sensors at 2 and 4 meters above ground (Laakso *et al*., 2012).

The HYSPLIT 2014 (Hybrid Single-Particle Lagrangian Integrated Trajectory) model was used for the calculation of air mass histories, i.e. back trajectories (Draxler & Hess, 2004). The time of the trajectories were corrected to reflect local time, since calculated trajectories were in Greenwich Mean Time (GMT). The Air Resources Laboratory (ARL) of the National Oceanic and Atmospheric Administration (NOAA) developed the HYSPLIT model. Meteorological inputs from the GDAS (Global Data Assimilation System) archive from the NCEP (National Centre for Environmental Prediction) and the USNWS (United States National Weather Service) were used. This data set was archived by the ARL (Air Resources Laboratory). A GDAS1 data set was used in this study as the GDASOP5 data set, with higher resolution, was not yet in use during the measurement period. However, according to Su (2014), the GDAS1 data set was accurate enough to determine the source locations of particulate

matter (PM) in complex source areas. The data set has a resolution of 1°×1° gridded cells with 23 vertical pressure layers (Air Resources Laboratory, 2014b). Hourly arriving back trajectories were calculated for 48 hours backwards, as this is estimated to be the approximate atmospheric lifetime of H_2S (Seinfeld & Pandis, 2006). The arrival heights of the back trajectories were set to 100 m above ground level, because the orography in HYSPLIT is not well defined (Air Resources Laboratory, 2014b). The error margin for an individual calculated trajectory is estimated to be at maximum between 15 to 30 percent of the total distance travelled (Stohl, 1998; Riddle, 2006). Therefore, by making deductions from multiple back trajectories, instead of a single trajectory, the chance of an error on a single trajectory to bias the result is significantly reduced.

3.3 Data cleaning and quality control/assurance

The collection of atmospheric measurements at Elandsfontein took place over a two-year period (from the beginning of February 2009 to the end of January 2011) during the EUCAARI project. Data gathering was only interrupted if maintenance, service and calibration of instruments were performed, or if power failures occurred (Laakso *et al.,* 2012).

The Elandsfontein measurement station was visited for regular maintenance at least once every ten days by staff from the Atmospheric Chemistry Research Group (ACRG) of the North-West University (NWU), accompanied by Eskom technicians. Maintenance conducted during these visits consisted of the inspection and adjustment of instrument flows, cleaning of inlets, and other procedures if necessary. An electronic diary of all site visits was kept, which was transferred daily, together with all measurement data, to a server to prevent the loss of information. The arrival and departure times of every site visit was logged, as well as the names of personnel visiting the site. The personnel names were important, since the site was maintained by several different people. If data/instrument abnormalities were identified later, the appropriate person could be consulted. All activities with associated time stamps were also recorded in the diary, even routine checks. Additionally, *ad hoc* maintenance procedures and abnormal observations (or events of interest, e.g. nearby open biomass burning event) were logged, since these were vital in understanding high/low concentrations of species monitored. The electronic diary also served as an institutional memory of how to solve problems that had occurred and had been resolved in the past (Laakso *et al.,* 2012; Beukes *et al.*, 2015).

The gas instruments were calibrated once every month and adjustments were made if necessary. Every three months, full maintenance of the station was carried out. This included more complicated service procedures such as the cleaning of measurement instrumentation cells. In addition to the site visits/checks, data that were downloaded onto the server was visually inspected for any irregularities

a few times per week. If any irregularities were found, an additional site visit was arranged to address the issue(s) as soon as possible (Laakso *et al.,* 2012; Beukes *et al.*, 2015).

The raw measurement data (one-minute resolution) were visualised and corrected by fit-for-purpose MATLAB scripts, as explained by Laakso *et al.* (2012) and Beukes *et al.* (2015). All data collected during site visits, which were logged in an electronic diary as indicated earlier, as well as artefacts caused by power failures (e.g. spikes or unstable measurements), were removed from the dataset. Data was then corrected based on zero and span, as well as flow checks. Multiple species were also visualised simultaneously with the aforementioned fit-for-purpose MATLAB scripts to enable manual detection of errors and/or suspicious data. For instance, if NO, CO and eBC peaked simultaneously, it confirmed the measurement of a fresh combustion plume. However, if only one of these species spiked (i.e. individual data point(s)), this suspicious data points(s) would be investigated further (e.g. by considering the electronic diary, other measured species/parameters and air mass histories). If no evidence could be found to support the validity of the suspicious data, it was removed from the data set.

After the data was corrected, it was averaged over 15-minute periods to compress the data set and provide a fit-for-purpose data set, which could then be used for further analysis (Laakso *et al.,* 2012; Beukes *et al.,* 2015). A 15-minute average was only calculated if at least two thirds of the one-minute resolution data points were available.

Chapter 4: Results and discussion

In this chapter, data coverage of the hydrogen sulphide (H_2S) data set collected at Elandsfontein is considered and the H_2S ambient concentrations contextualised (Par. 4.1). Thereafter, in Par. 4.2, the temporal patterns of H_2S measured at Elandsfontein are discussed. Par. 4.3 and 4.4 present the developed source apportionment method and different case studies on how the sources were differentiated. In Par. 4.5, the source apportionment of H_2S is discussed, which is followed by the conclusion in Par. 4.6.

4.1 Data coverage and contextualisation

For H_2S specifically, which is the species of interest in this study, a total of 52 512 instances of 15-minute averages was calculated, after data cleaning (Par 3.2), out of a possible 70 080 averages over the two-year measurement period. This gives a H_2S data coverage/availability of 74.9% (approximately 75%). Most of the data gaps were due to electrical power outages, since South Africa was plagued by an energy crisis at the time (Pretorius *et al.,* 2014). Additionally, data points of which the quality was questionable/uncertain were removed to ensure a high-quality data set, as per the data cleaning and quality control procedures presented in Par. 3.2. Considering that most of the data gaps were due to power outages and that the data set was thoroughly cleaned/quality verified, the 75% data coverage can be considered as good. Additionally, data gaps were distributed throughout the measurement period and not concentrated in certain times/periods, therefore avoiding bias in the data set.

In Table 4.1, the mean and median, as well as 5^{th}, 25^{th}, 75^{th} and 95^{th} percentile concentration values for the entire study period are presented. The mean H_2S concentration of 3.1 ppb was significantly higher than mean concentrations reported for true background sites such as over the northern equatorial Atlantic Ocean and rural regions of France where mean H_2S concentrations of 5 to 50 ppt (0.000005 to 0.00005 ppb) and 0.055 ppb were respectively recorded (Slatt *et al.,* 1978; Delmas *et al.,* 1980). The mean of 3.1 ppb was comparable to means reported for an urban site in Greece where the average concentration of H_2S was 5.55 ppb in the city of Thessaloniki (Kourtidis *et al.,* 2007) and to a residential area in Arkansas close to gas processing plants where mean concentrations of 2.4 and 3.4 ppb were recorded for May to July and October to December 1998, respectively (Skrtic, 2006). However, the mean H_2S concentration at Elandsfontein was significantly lower than the means reported for heavily H_2S polluted sites such as Whakarewarewa Village in the city of Rotorua in New Zealand. Here, a mean range of 66 to 100 ppb was recorded (Petersen *et al.,* 1998; Wegmuller & Peterson, 1998; Hinz, 2011), due to the proximity of an active geothermal field.

Table 4.1: Mean and median, as well as the 5th, 25th, 75th and 95th percentile concentration values for H_2S over the entire measurement period

Description	Value (ppb)
Mean	3.1
Median	1.8
5th Percentile	0.4
25th Percentile	1.1
75th Percentile	3.2
95th Percentile	11.1

As previously stated, there is currently no South African National Ambient Air Quality Standard (NAAQS) for ambient atmospheric H_2S. However, the South African Department of Environmental Affairs (DEA) stipulates that if in any day a one hourly average H_2S concentration exceeds 29 ppb, this day is regarded as a high H_2S day (DEA, 2009). The calculated hourly average H_2S levels exceeded this 29 ppb "standard" 47 times, as indicated in Table 4.2. These "exceedances" occurred only on 13 days, therefore only 13 "high H_2S days" were recorded at Elandsfontein during the two-year measurement period.

Table 4.2: Table of one-hour average exceedances of the "high day" 29 ppb "standard" according to the DEA (2009)

Date of exceedance	Time of exceedance	Average concentration (ppb)	Date of exceedance	Time of exceedance	Average concentration (ppb)
2009/04/18	02:00-03:00	34.9	2009/09/18	10:00-11:00	48.6
2009/04/24	05:00-06:00	36.7	2009/12/18	04:00-05:00	46.8
2009/04/24	06:00-07:00	30.9	2009/12/23	01:00-02:00	36.3
2009/04/24	08:00-09:00	33.3	2009/12/23	02:00-03:00	30.3
2009/04/25	01:00-02:00	31.8	2010/05/24	02:00-03:00	33.4
2009/05/16	04:00-05:00	31.3	2010/05/24	14:00-15:00	32.0
2009/05/19	13:00-14:00	34.9	2010/05/24	15:00-16:00	42.3
2009/05/19	14:00-15:00	33.9	2010/05/24	16:00-17:00	38.6
2009/06/01	09:00-10:00	66.7	2010/06/05	14:00-15:00	52.3
2009/06/01	10:00-11:00	68.2	2010/06/05	15:00-16:00	60.8
2009/06/01	11:00-12:00	52.1	2010/06/05	16:00-17:00	44.7
2009/06/01	12:00-13:00	39.8	2010/06/05	17:00-18:00	32.2
2009/06/03	00:00-01:00	34.4	2010/06/06	15:00-16:00	33.5
2009/06/28	09:00-10:00	37.4	2010/06/06	16:00-17:00	33.6
2009/06/28	10:00-11:00	74.6	2010/06/08	05:00-06:00	71.6
2009/06/28	13:00-14:00	41.0	2010/06/21	20:00-21:00	30.8
2009/06/28	14:00-15:00	32.2	2010/06/21	21:00-22:00	31.3
2009/07/02	01:00-02:00	29.8	2010/06/23	00:00-01:00	36.4

Table 4.2 cont.: Table of one-hour average exceedances of the "high day" 29 ppb "standard" according to the DEA (2009)

Date of exceedance	Time of exceedance	Average concentration (ppb)	Date of exceedance	Time of exceedance	Average concentration (ppb)
2009/07/03	02:00-03:00	38.7	2010/06/23	03:00-04:00	33.5
2009/07/09	12:00-13:00	29.5	2010/07/16	09:00-10:00	30.0
2009/07/10	19:00-20:00	37.4	2010/08/14	11:00-12:00	32.8
2009/07/12	23:00-24:00	42.0	2010/09/27	09:00-10:00	31.4
2009/08/20	09:00-10:00	42.1	2010/11/20	10:00-11:00	53.5
2009/09/15	22:00-23:00	32.4			

4.2 Temporal H_2S patterns

Statistical distribution of monthly H_2S concentrations measured at Elandsfontein are presented in Figure 4.1 as box and whisker plots – for referencing purposes, the numerical values presented in this figure are given in Appendix A, Table 4.3. It is evident from Figure 4.1 that H_2S concentrations were in general higher in the colder and/or dryer months and lower in the wetter/hotter months. This indicates that low-level emission sources likely make a significant contribution to ambient H_2S measured at Elandsfontein, since such emissions can be trapped and concentrated by low-level thermal inversion layers and/or a shallow planetary boundary layer (PBL) depth (Garstang *et al.,* 1996; Korhonen *et al.,* 2014; Gierens *et al.,* 2019). These conditions are particularly common over the South African Highveld during night-time and early mornings of the colder months (Garstang *et al.,* 1996; Korhonen *et al.,* 2014; Gierens *et al.,* 2019) and reduce vertical mixing in the troposphere.

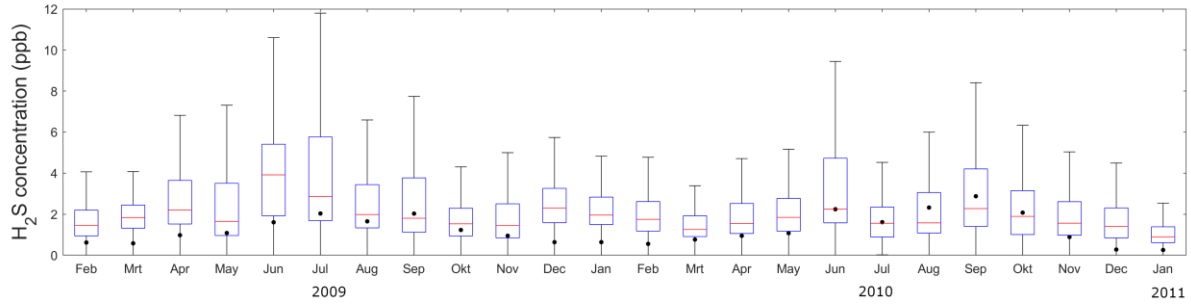

Figure 4.1: Box and whisker plots of the measured H_2S concentrations for each month during the study period. The red line represents the median, the black dot the mean, the box the 25th and 75th percentiles and the whiskers are 1.35 times the standard deviation which represents 99.3% data coverage if a Gaussian/normal distribution is assumed.

In Figure 4.2, the overall diurnal pattern (for the entire measurement period), as well as diurnal patterns for the different seasons are depicted. From this figure it is evident that H_2S concentrations were highest in winter (red line), which correlates with the seasonal analysis considered in Figure 4.1. In general, the diurnal patterns are characterised by bimodal peaks, occurring in the early morning

(between approximately 04:00 and 08:00) and evening (after approximately 19:00), which again support the notion of low-level emissions being trapped by inversion layers and/or a low PBL depth (Garstang *et al*., 1996; Korhonen *et al*., 2014; Gierens *et al*., 2019), as explained in Par.4.1. A relatively prominent peak is also observed between 9:00 and 13:00 in all the diurnal patterns, which is indicative of high stack emissions mixing down to the surface after the break-up of the aforementioned inversion layers and growth of the PBL (Garstang *et al*., 1996; Korhonen *et al.,* 2014; Gierens *et al*., 2019). This peak is particularly strong in winter due to thermal inversion layers being more prominent and stronger and the PBL depth being lower during this time than in the hotter months.

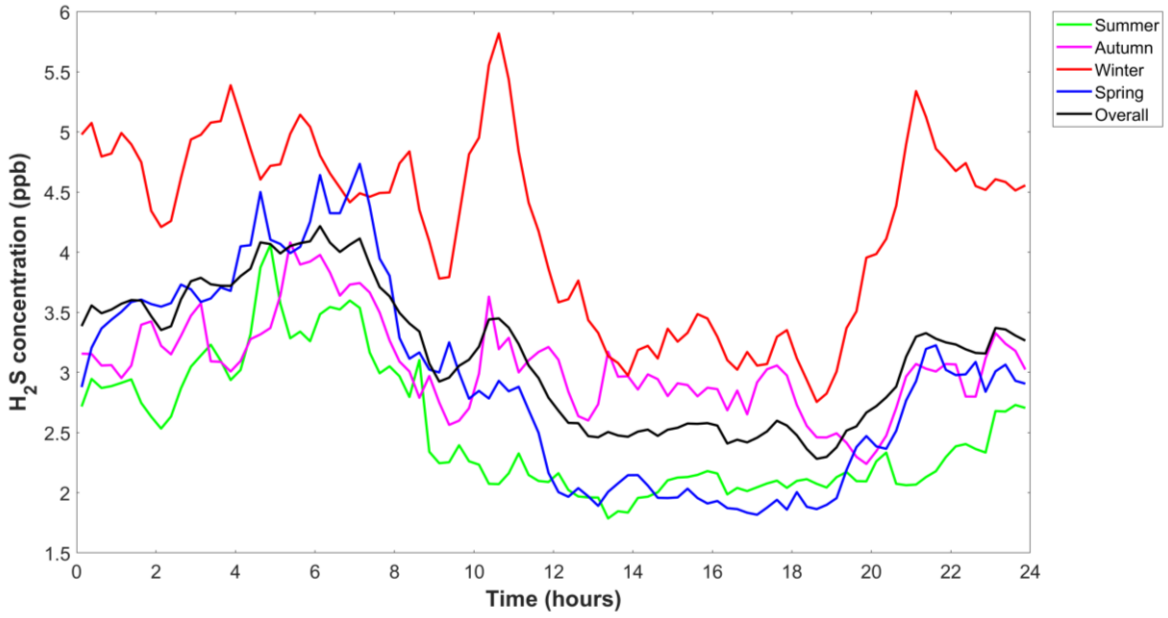

Figure 4.2: 15 min average diurnal patterns of H_2S for the entire measurement period, as well as separate average patterns for each season.

4.3 Development of novel source apportionment method

Although some general H_2S source insights were gained from the temporal patterns presented in Par. 4.2, source apportionment was not possible. Historically, source apportionment of ambient atmospheric concentrations in South Africa have mainly been conducted with two techniques. The first method is source modelling using emission factors of sources and/or gridded emission quantities to simulate actual ambient concentrations (Par. 2.1). Once this is achieved, sensitivity analysis can be conducted (e.g. in/excluded source(s) or altering meteorological conditions) to assess the effect thereof (e.g. Zunckel *et al*., 2000; Kuik *et al*., 2015; Lourens *et al*., 2016). The second method is receptor modelling where the ambient concentrations are measured, where after possible source contributions are calculated based on source profiles, chemical mass balances, and/or multivariate

calculations, e.g. principal component analysis (PCA) and positive matrix factorisation (PMF) (Par. 2.1) (e.g. Engelbrecht *et al*., 2002; Conradie *et al*., 2016; Venter *et al*., 2017; Jaars *et al*., 2018).

Of particular relevance in this study is receptor modelling. Most such studies for South Africa have primarily focused on particulate matter (PM) and/or wet deposition without considering trace gases (e.g. Maenhaut *et al*., 1996; Engelbrecht *et al*., 2002; Mphepya *et al*., 2004 and 2006; Van Zyl *et al*., 2014; Tiitta *et al*., 2014; Conradie *et al*., 2016; Venter *et al*., 2017; Jaars *et al*., 2018). This is due to most receptor source apportionment techniques being more ideal for PM and/or wet deposition applications (Hopke, 2008), which enables relatively straightforward statistical analysis with PCA, PMF and CMB. Considering the regular exceedances of ambient air quality standard limits for criteria trace gases (DEA, 2009) in the Highveld Priority Area (DEA, 2010) (Par. 2.2), it is necessary to also conduct receptor source apportionment for these species.

To partially address shortcomings in the current receptor modelling methodologies, a novel technique to conduct source apportionment on continuously measured trace gasses was developed by modifying and improving a method that was relatively recently presented by Chiloane *et al.* (2017). The afore-method related continuous eBC concentrations measurements at a specific receptor site to possible sources, by considering co-incidental concentration changes and air mass histories. However, this method only considered the larger point sources (e.g. petrochemical operations, pyro-metallurgical smelter, coal-fired power stations) and did not account for smaller area sources (Chiloane *et al*., 2017). Another weakness of the method is that it was very labour intensive and required separate scripts (programs) to be run in succession to conduct source apportionment.

To facilitate the explanation of the technique, the developed algorithm is presented in Figure 4.3. This algorithm has been programmed as a MATLAB script, but any similar programming language (e.g. R, Python) could be used.

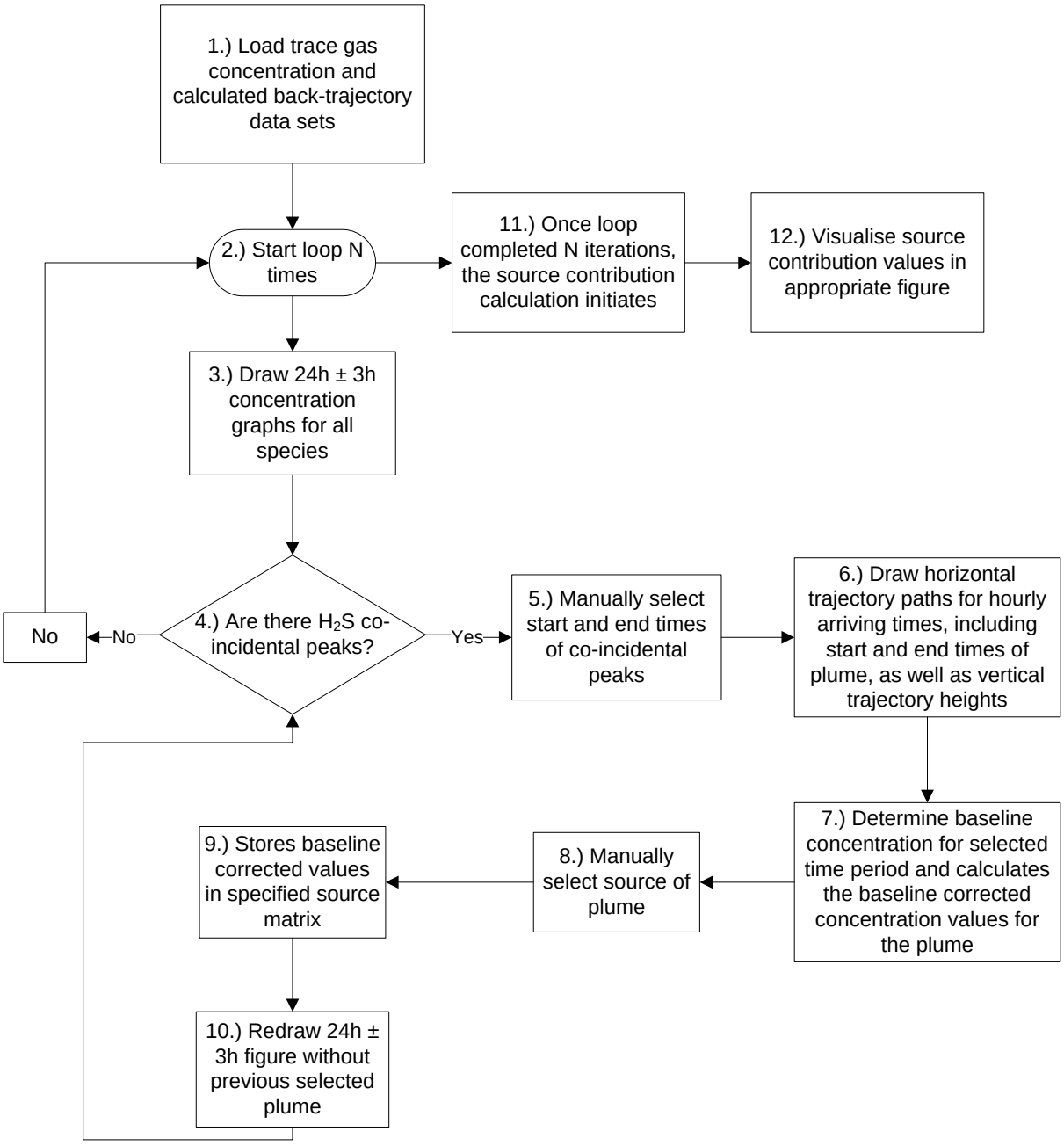

Figure 4.3: Algorithm (flow diagram) for the novel source apportionment method developed.

The steps indicated in the algorithm (Figure 4.3) are discussed in more detail below.

1) In the first step, the relevant data sets are loaded. In this case the Elandsfontein data set, acquired during the EUCAARI project (Laakso *et al*., 2012; Par. 3.2), as well as hourly arriving back trajectories (Par. 3.4) calculated for the entire measurement period, were loaded.
2) Thereafter, a loop starts iterating N times, with N the number of days (i.e. 24hr periods) in the data set. In the current study the start day was 1 February 2009 and the end day 31 January 2011 (Par 3.1 and 3.2).

3) In the next step, 24hr ± 3hr concentration *vs*. time graphs for all the relevant species considered are plotted. Example 24hr ± 3hr graphs, indicating the concentrations of nitrogen oxide (NO), nitrogen dioxide (NO_2), sulphur dioxide (SO_2), H_2S and equivalent black carbon (eBC, definitions according to Petzold *et al.,* 2013) are presented in Figure 4.4. The receptor modelling technique developed is based on the identification of co-incidental concentration peaks. Therefore, to ensure that a peak that extends over two consecutive days is correctly identified as a single peak, the ± 3hr periods are drawn with the specific 24hr period considered.

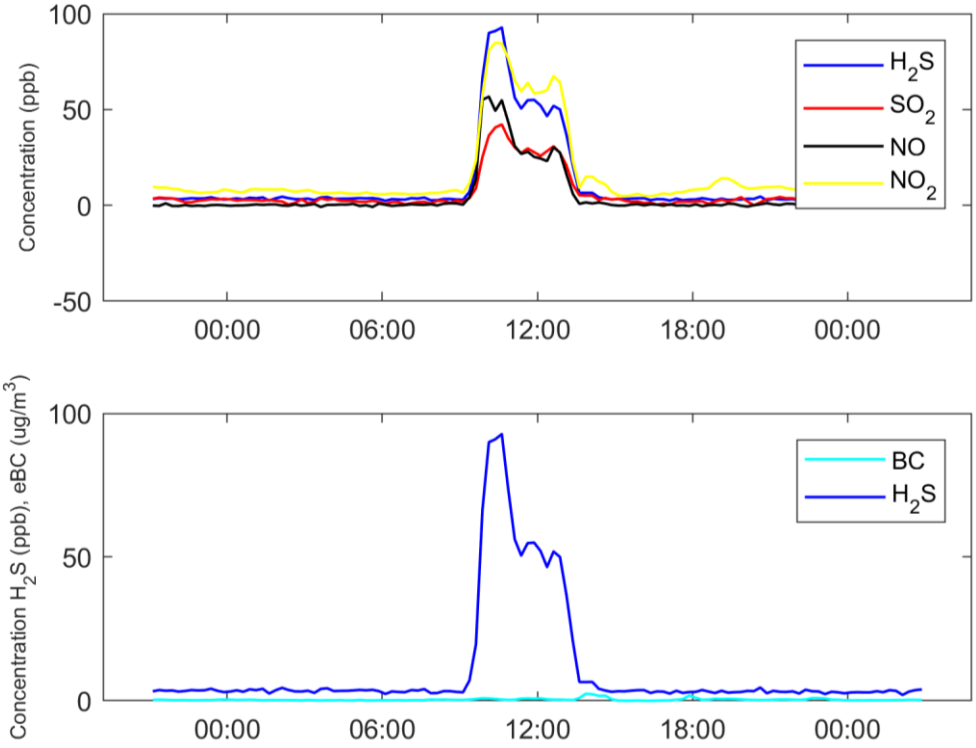

Figure 4.4: Examples of 24hr ± 3hr concentration vs. time graphs for H_2S, SO_2, NO, NO_2 and eBC on 1 June 2009.

4) In the next step the user must make a choice, by answering "y" (for "yes") or "n" (for "no") to the question "Are there H_2S co-incidental peaks?" Unfortunately, user input such as this, is required. In this particular step, only peaks that could clearly be identified from the measurement noise were considered. If "n" is selected, the program returns to step 2 and the next iteration of the loop starts. However, if "y" is selected, the program proceeds to step 5.

5) The user must now select the start and end times of one of the observed co-incidental peaks. As is evident from the example presented in Figure 4.4, there was a well-defined co-incidental peak from 09:07:30 to 13:35:30 (format HH:MM:SS), where H_2S peaked at the same time as NO, NO_2 and SO_2. In the particular data set used, the 15-min. average

concentrations were stored in the midpoint of each 15-min average, hence the somewhat "strange" time stamps (HH:MM:SS). Although the example figure presented here is relatively small (Figure 4.4), the figures fill the entire screen in the actual program. The aforementioned times are therefore relatively easily selected by clicking with the mouse close to the peak start and stop times, with the program automatically selecting the nearest 15-min. time stamps.

6) After selection of the co-incidental peak identified in step 5, 2 figures (Figures 4.5 and 4.6 as examples) are automatically plotted to help the user classify/attribute the plume to the correct source. Figure 4.5 depicts the horizontal back trajectory paths of all hourly arriving back trajectories during the plume period that was selected in step 5, while Figure 4.6 indicates the corresponding vertical heights of the trajectories. For the example plume indicated here, 5 calculated hourly arriving back trajectories were drawn. The trajectory lines are in different colours to help differentiate them from one another. As indicated earlier (Par. 3.4), consideration of such multiple trajectories significantly reduces the risk of wrong deductions based on a single trajectory. Although not relevant in the specific example presented in Figure 4.5 (due to relatively fast air mass movement), the first 24hrs of the trajectories are indicated by the different colour lines, while the period 25 to 48 hrs backward are indicated with black lines. This is done to visually help the user assess the potential age of emissions, which is important since the atmospheric lifetime of H_2S is approximately 48 hrs (Seinfeld & Pandis, 2006). Trajectory heights (Figure 4.6) are also important, since they help the user to, for instance, differentiate between industrial high stack emissions (e.g. H_2S from petrochemical operation and coal-fired power stations) and ground level emissions (e.g. H_2S from waste water facilities, solid waste dumps and feedlots).

7) Although indicated as a separate step, the program calculates the baseline H_2S concentration and baseline corrected plume concentrations for the selected plume period simultaneously with step 6. The baseline value is calculated as the average between the start and end concentrations of the plume, while the plume baseline corrected concentrations are calculated by subtraction of the baseline value from each 15-min average concentration during the selected plume period.

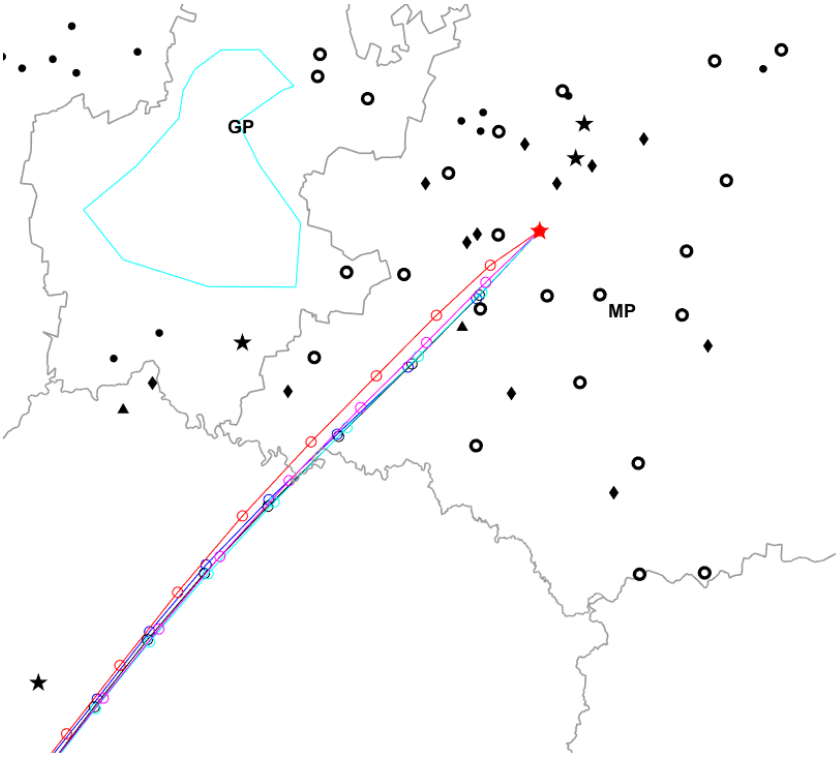

Figure 4.5: Horizontal back trajectory paths for the selected example of a co-incidental H_2S peak depicted in Figure 4.4.

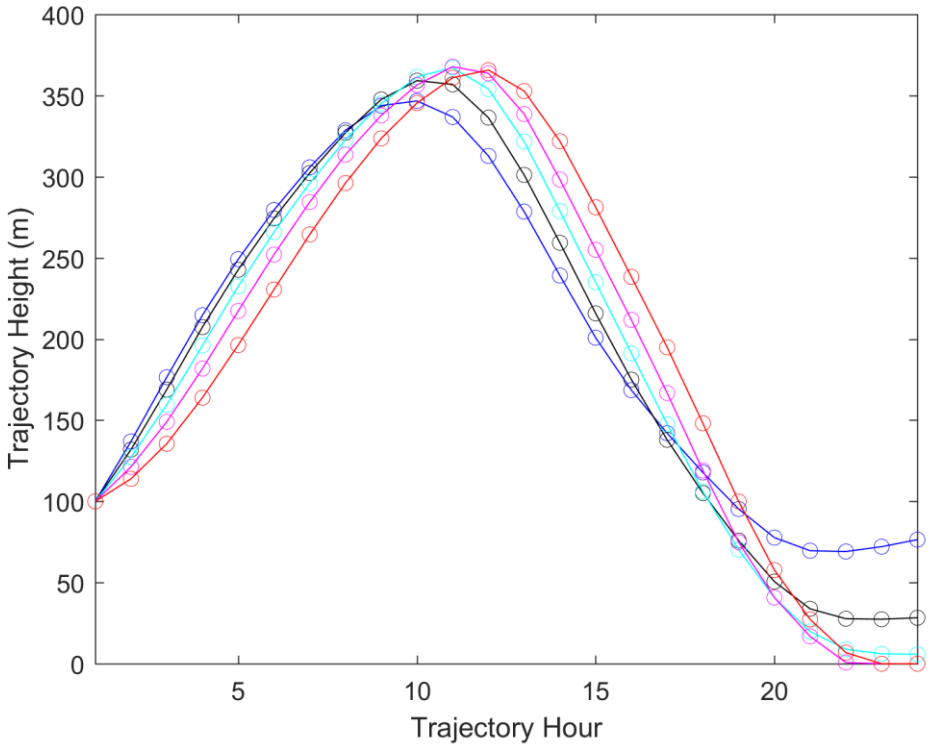

Figure 4.6: Calculated vertical trajectory heights corresponding to the calculated horizontal trajectory paths presented in Figure 4.5.

8) The user now has to manually attribute the plume to the correct source by selecting the corresponding number from a list of different sources. For H_2S, the potential sources from which can be selected include the petrochemical operation near Secunda, coal-fired power stations, pyrometallurgical smelters, the Johannesburg-Pretoria (Jhb-Pta) megacity, feedlots, the paper mill near Nelspruit, emissions associated with towns/small cities/informal and semiformal settlements (which include waste water treatment facilities, landfills, household combustion emissions, small industries and vehicle emissions, especially from older diesel engines) and mixed/undefined sources. This selection is done by considering all the relevant information depicted in Figures 4.4 to 4.6. For instance, co-incidental increases in certain species can be expected from certain sources (Figure 4.4) and different sources might have different plume amplitude strengths. The source assumption can also be confirmed by considering the corresponding trajectory information (Figures 4.5 and 4.6). For the specific plume example presented in Figures 4.4 to 4.6, it could be deduced that the measured H_2S plume originated from the petrochemical operation near Secunda. This was firstly indicated by the relatively large plume amplitude, which is not to be expected for area sources. Secondly, the co-incidental increase in H_2S concentration with NO, NO_2 and SO_2, but not eBC (Figure 4.4), supported this deduction – the petrochemical operation generates a significant fraction of its own electricity, therefore NO, NO_2 and SO_2 emissions will coincide with H_2S. Additionally, Chiloane *et al*. (2017) proved that the specific petrochemical operation considered here did not significantly contribute to eBC measured at Elandsfontein, therefore the absence thereof in this plume makes sense. Thirdly, the calculated back trajectories during the plume period passed very close to the petrochemical operation. Lastly, the timing of the identified plume corresponds to a typical high stack emission that mixes down to surface after the breakup of the low-level inversion layer(s), which typically occurs between 08:00 and 10:00 as the depth of the planetary boundary layer (PBL) starts to increase at Elandsfontein (Korhonen *et al*., 2014). In addition to the petrochemical associated plume example considered here (Figures 4.4 to 4.6), more examples in the form of case studies of different sources are presented in Par. 4.4.

9) Once the source is identified, the plume baseline corrected concentration values of H_2S are stored in the data matrix for that particular source. For the example plume considered here (Figure 4.4), 19 plume baseline corrected 15-min. average concentration values (09:07:30 ≤ period ≤ 13:35:30) were stored in the source matrix of the petrochemical operations.

10) In this step the program redraws the considered concentration *vs*. time 24h ± 3h period graphs, as indicated in Figure 4.7. However, in these graphs the previously attributed plume

concentrations are replaced with the baseline value calculated in step 7 and the y-axes of the graphs (species concentrations) are rescaled to enable easier identification of possible smaller co-incidental peaks.

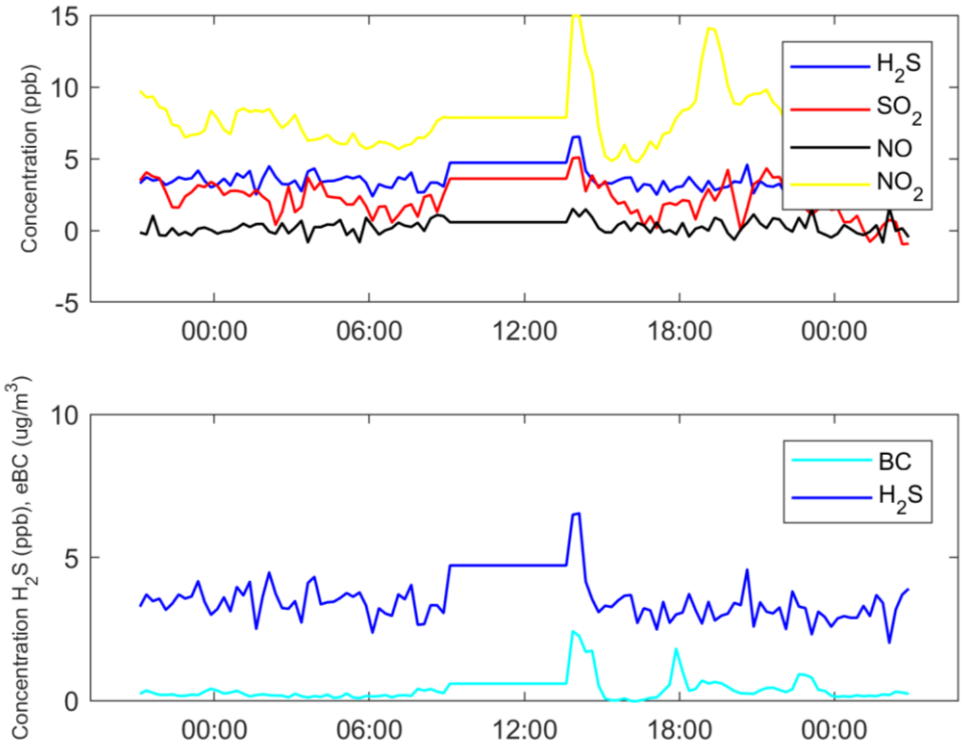

Figure 4.7: 24hr ± 3hr concentration vs. time graphs for H_2S, SO_2, NO, NO_2 and eBC of 1 June 2009, with the previously selected H_2S and other co-incidental peaks (identified in Figure 4.4) replaced by the baseline value.

4) The program then returns to step 4, where the user again must answer "y" (for "yes") or "n" (for "no") to the question "Are there H_2S co-incidental peaks?" If there is one or more coincidental peak(s) in the particular 24hr ± 3hr period, the entire process is repeated (steps 3 to 10), until all such peaks have been attributed to sources. As soon as the user answers "n" (for "no") to the question in step 4, the next iteration (next 24hr ± 3hr period) is considered in the same manner. The process is repeated until all the co-incidental peaks throughout the entire sampling period have been attributed to sources.

11) Once all iterations are completed, the source contribution calculation initiates (step 11). In this calculation, Equation 4.1 is applied to each of the source matrices. This equation calculates the percentage contributions to ambient H_2S measured at Elandsfontein for each of the identified sources.

$$\%\ Source\ contribution = \frac{Cs}{Tc} \qquad (4.1)$$

where C_s is the sum of all the plume baseline concentration values that were attributed to the specific source; and T_c is the sum of all the plume baseline concentrations that were

attributed to all the source matrices. Additionally, the background/baseline H_2S concentration for the entire measurement period is also calculated from the average concentrations remaining after all attributed plume concentrations have been replaced by the plume-specific baseline values.

12) Finally, an appropriate figure (and table with actual values) is drawn to visualise the H_2S source apportionment. This figure for H_2S source apportionment at Elandsfontein, over the two-year measurement period considered in this study, is presented and discussed in Par. 4.6.

4.4 Case studies for different sources

In this section, example case studies will be presented to illustrate how the different sources were distinguished. As indicated earlier, sources were differentiated on the basis of:

- Emission profiles of pollutant species, since different sources emit different combinations of species. Therefore, co-incidental concentration profiles were a key indicator.
- Time of day that the peaks were observed, which could help differentiate high stack- and low-level emission sources. This is due to low-level inversions and the shallow PBL during the evening and early mornings that prevent vertical mixing, especially during the colder periods (Garstang *et al*., 1996; Korhonen *et al*., 2014; Gierens *et al*., 2019). Therefore, high stack emissions were unlikely to be detected during times when atmospheric stratification was strong, while low-level emission sources were very common during that time.
- Concentration peak duration and amplitude. Firstly, plumes from large point sources are typically shorter in duration, since a shift in wind direction results in the plume not being detected, while area sources are less affected by wind direction due to the larger surface area of such sources. Secondly, plumes from large point sources typically have larger concentration amplitude differences, while more defuse area sources are indicated by smaller amplitude differences.
- Horizontal and vertical back trajectory paths. The horizontal back trajectory path can be used to confirm that an air mass associated with a co-incidental peak has passed over or close to a specific source(s) and the trajectory height can additionally be used to confirm the height of the emission.

4.4.1 Case study for the petrochemical operation near Secunda

In Section 4.3, a detailed description of an H_2S plume originating from the petrochemical operation near Secunda was given. An additional case study is presented here. For this specific petrochemical operation, an increase in H_2S, SO_2, NO_2 and NO, but not eBC, is expected, (Chiloane *et al*., 2017). In Figure 4.8, a simultaneous increase in the aforementioned species can be observed between 08:00 and 11:00 on the 16th of July 2010. The amplitude and timing of the co-incidental peaks suggest a high stack emission source. It is not expected for an area source to have such a significant plume amplitude

and the observation time of the identified plume is after the break-up of thermal inversion layers and growth of the PBL depth, which allow the high stack emissions to mix down to the surface (Garstang *et al*., 1996; Korhonen *et al*., 2014; Gierens *et al*., 2019), as discussed in Par. 4.2.

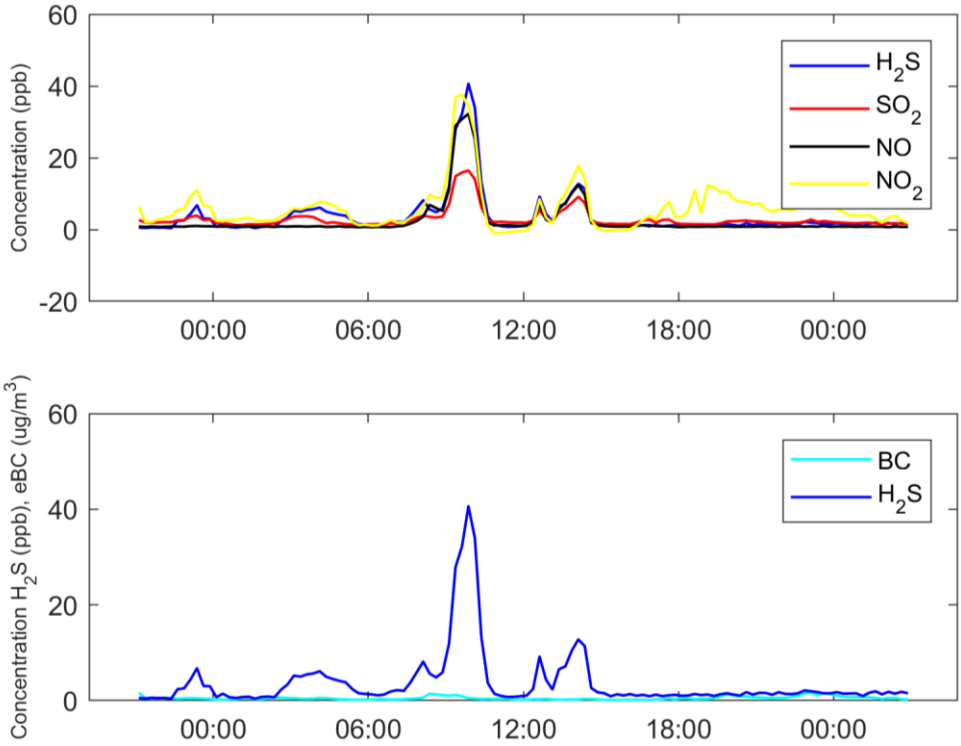

Figure 4.8: 24hr ± 3hr concentration vs. time graphs of co-incidental increases of H_2S, SO_2, NO, NO_2, but not eBC for the 16th of July 2010.

From the back trajectory heights (Figure 4.9a) and horizontal back trajectory paths (Figure 4.9b) for the selected period, one can see that the air masses travelled over the petrochemical operation near Secunda (black triangle) at a high altitude. From all information depicted in Figures 4.8 and 4.9, it is evident that the co-incidental concentration peaks between 08:00 and 11:00 are high stack emissions that originated from the petrochemical operation near Secunda.

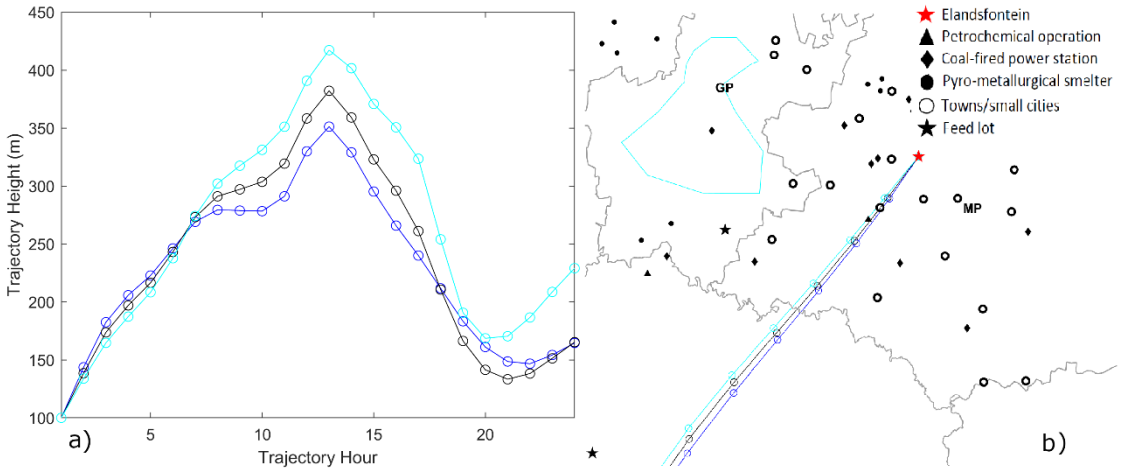

Figure 4.9: a) Calculated vertical back trajectory heights. b) Horizontal back trajectory paths arriving on the hour for the identified plume in Figure 4.8, corresponding to the calculated trajectory heights.

4.4.2 Case study for a pyrometallurgical smelter

Plumes from pyrometallurgical smelters on the Mpumalanga Highveld in the Middelburg/Witbank area are usually characterised by coincidental increases of SO_2, NO_2 and eBC, together with H_2S (Chiloane *et al.,* 2017). H_2S is present in such plumes, since pyrometallurgical smelting is a reductive process, which enhances H_2S formation. However, a significant fraction of the H_2S will be oxidised to SO_2 during off-gas combustion either in the open or semi-closed furnaces (Beukes *et al*. 2017), or during flaring of cleaned off-gas (Du Preez *et al.,* 2015; Beukes *et al*., 2017). In Figure 4.10, the co-incidental increase of H_2S, SO_2, eBC and some NO_2 is observed between 04:00 and 10:00 on the 24th of April 2009, which is the first indication that this plume might have originated from a pyrometallurgical smelter.

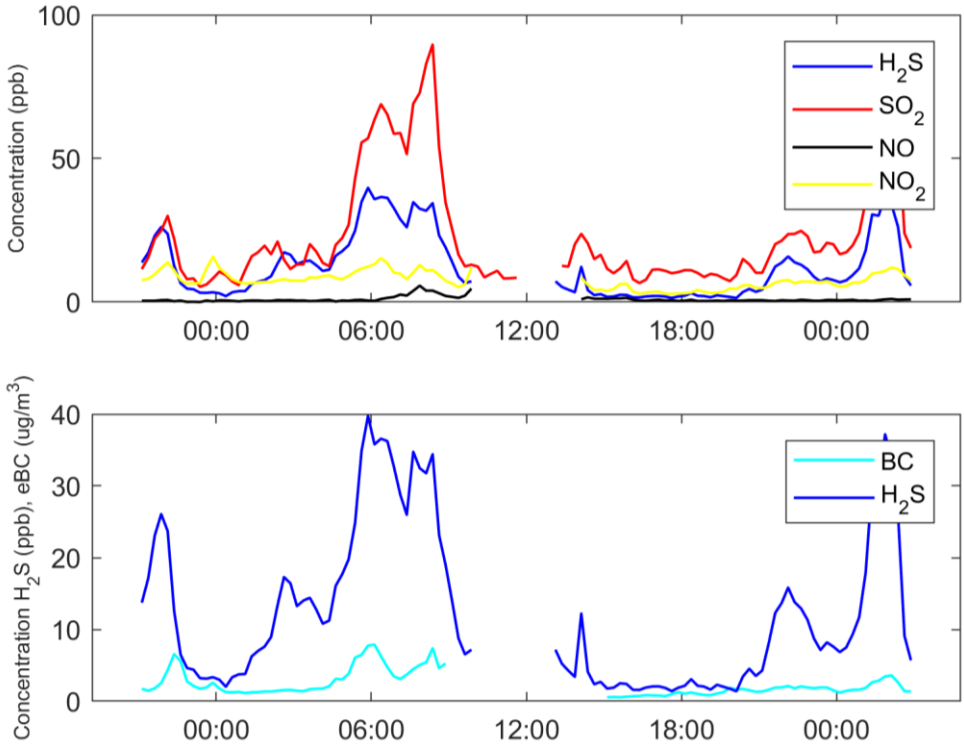

Figure 4.10: 24hr ± 3hr concentration vs. time graphs of co-incidental increases of H_2S, SO_2, NO, NO_2 and eBC for the 24th of April 2009.

One would expect emissions from pyrometallurgical smelters to be released *via* high-stacks. However, in South Africa the stacks of pyrometallurgical smelters are typically not very tall. For example, the highest stack at Glencore's Lion Ferrochrome smelter in Steelpoort is 58m and on average the stacks at this smelter are just 45m tall (Airshed Planning Professionals, 2004). According to the Rustenburg Local Municipality air quality management plan (Piketh *et al*., 2005), only some platinum group metal (PGM) smelters have stacks that are >100m tall, while most other smelters typically have stacks lower than 50m. PGM smelters emit significant quantities of SO_2 since they consume sulphide-rich ore (Xiao & Laplante, 2004). However, on the Mpumalanga Highveld there are no PGM smelters, just Ferrochrome, Ferromanganese and Ferrovanadium smelters, as well as a steel mill. Therefore, these pyrometallurgical smelters will emit pollutants beneath the stable nocturnal PBL and/or low-level thermal inversion layers, where it can be trapped and concentrated at night-time and during early mornings. Plumes from these smelters could therefore be observed at Elandsfontein during any time of the day, although night-time and early morning plumes would be expected to exhibit higher pollutant concentrations because they are trapped near the surface.

In Figure 4.11a, it is observed that the calculated back trajectories for this specific case study plume passed over three pyrometallurgical smelters that are located in the Witbank area. Additionally, these trajectories remained beneath the typical depth of the stable nocturnal PBL (Figure 4.11a). This, and

the indicators presented in the preceding two paragraphs, prove that this specific case study plume originated from the pyrometallurgical smelters in the Witbank area.

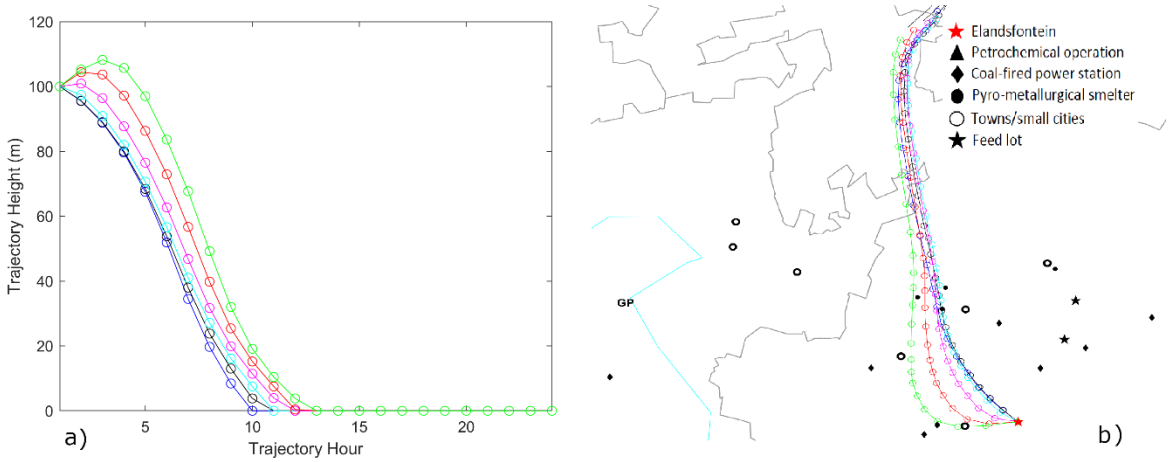

Figure 4.11: a) Calculated vertical back trajectory heights. b) Horizontal back trajectory paths arriving on the hour for the identified plume in Figure 4.10, corresponding to the calculated trajectory heights.

4.4.3 Case study for coal-fired power stations

It was not expected to observe significant H_2S emissions associated with coal-fired power station plumes at Elandsfontein, as boilers at these facilities burn (which is an oxidation process) at exceptionally hot temperatures. The temperature inside the boilers is approximately 1200°C at full load (ESKOM, 2019). Therefore, at full load, the reductive conditions required for H_2S formation is extremely unlikely. However, H_2S was observed in some coal-fired power station plumes, hence two case studies are presented. The first will be a normal (more common) coal-fired power station plume, without H_2S being observed, and the second, a less commonly observed coal-fired power station plume with H_2S being present. The reason for the presence of H_2S in some coal-fired power station plumes will be discussed with the latter case study.

Coal-fired power station plume without H_2S

Typically, plumes associated with high stack coal-fired power generation emissions in the South African interior are observed at ground level after growth of the stable nocturnal PBL and/or breakup of low-level thermal inversion layers in the morning. This often results in a sharp increase in pollutant concentrations as downward mixing occurs (Par. 4.2 and Figure 4.2). Such a plume is visible in Figure 4.12, where a sharp increase in SO_2, NO_2 and NO, but not H_2S, was observed between 09:00 and 12:00 on the 14th of February 2009. These species, i.e. SO_2, NO_2 and NO, suggest a coal-fired power station origin (Collet *et al.,* 2010; Lourens *et al.,* 2011).

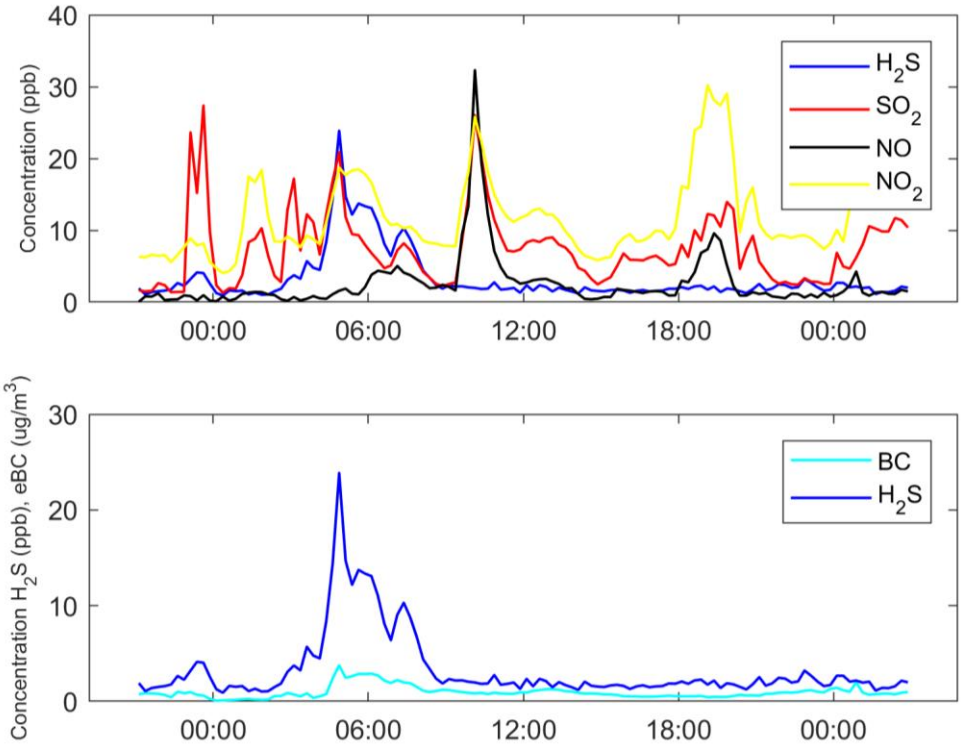

Figure 4.12: 24hr ± 3hr concentration vs. time graphs of co-incidental increases of SO_2, NO and NO_2 between 09:00 and 12:00 on the 14th of February 2009.

Furthermore, in Figures 4.13 (a and b), it is observed that the back trajectories of this specific plume passed over two coal-fired power stations, and that the trajectories passed over these point sources at heights similar to the expected emission heights. Taking into account the co-incidental increases of NO, NO_2 and SO_2, the timing and amplitude of the co-incidental increases, and trajectory paths and heights, it is evident that the plume originated from a coal-fired power station(s).

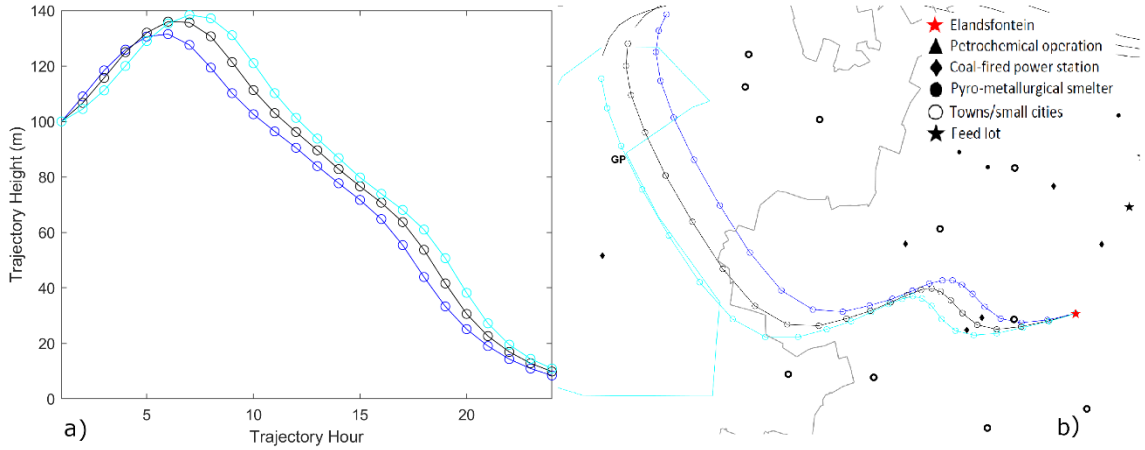

Figure 4.13: a) Calculated vertical back trajectory heights. b) Horizontal back trajectory paths arriving on the hour for the identified plume in Figure 4.12, corresponding to the calculated trajectory heights.

Coal-fired power station plume with H_2S

As indicated in Figure 4.14, coincidental increases in SO_2, NO_2, NO and H_2S were observed between 10:00 and 14:00 on the 16th of March 2009. As explained earlier, the timing and amplitude of the co-incidental peak suggest that the plume is of high stack origin, i.e. either from a coal-fired power station or the petrochemical operation near Secunda.

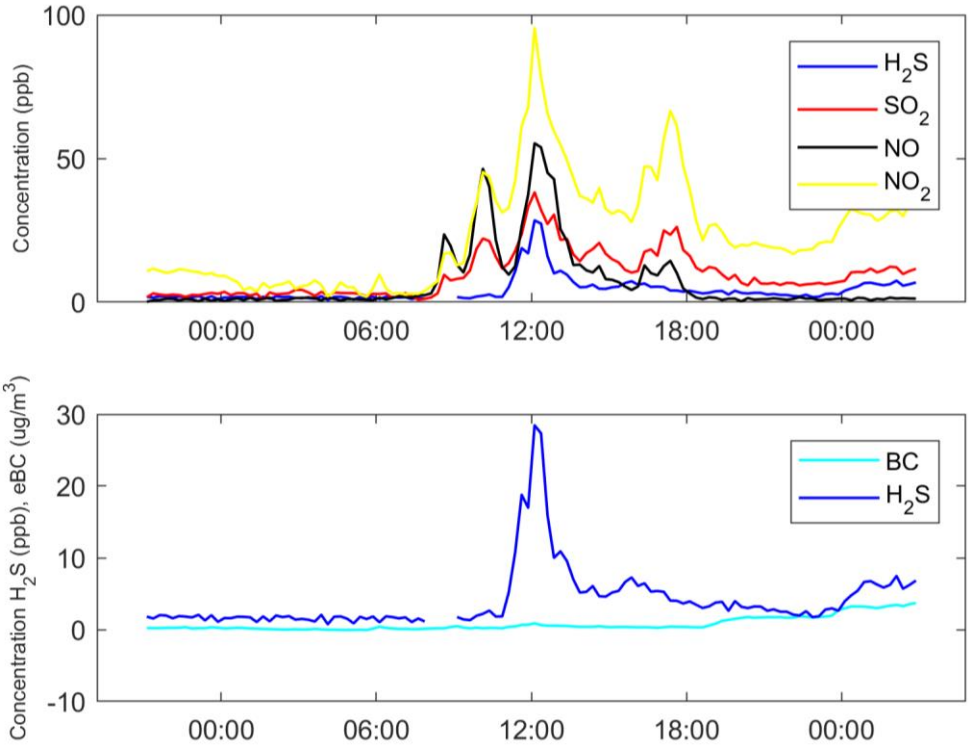

Figure 4.14: 24hr ± 3hr concentration vs. time graphs of co-incidental increases of H_2S, SO_2, NO and NO_2 on the 16th of March 2009.

Because of the presence of H_2S in the co-incidental peaks considered in this case study (Figure 4.14), it could be assumed that the plume originated from the petrochemical operation. However, by considering the horizontal back trajectory paths and heights (Figures 4.15a and b), it is clear that this plume did not originate from the petrochemical operation near Secunda. From the trajectory paths, it is evident that the air masses travelled close to a coal-fired power station south-east of the Elandsfontein measurement site (Figure 4.15b). The trajectory heights also indicate high stack emissions (Figure 4.15a). Thus, the point of origin for this plume is a coal-fired power station.

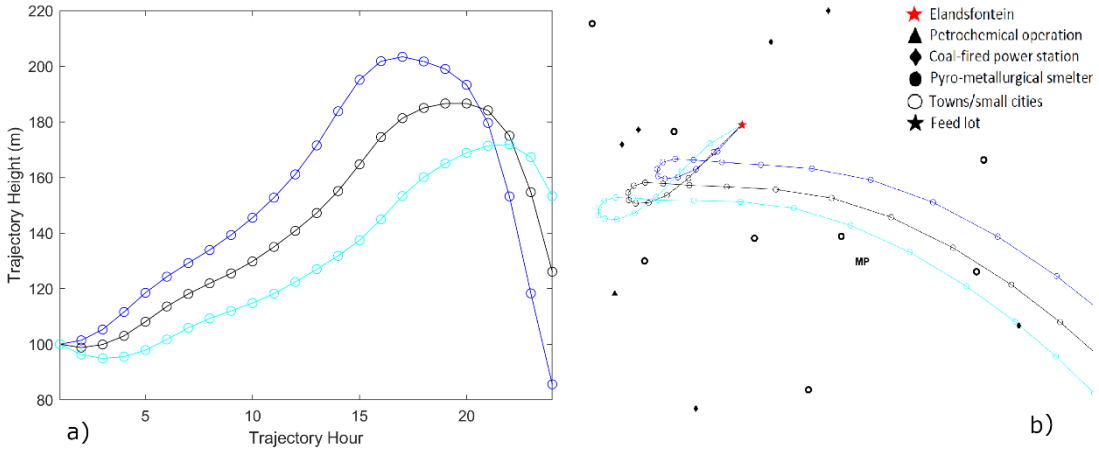

Figure 4.15: a) Calculated vertical back trajectory heights. b) Horizontal back trajectory paths arriving on the hour for the identified plume in Figure 4.14, corresponding to the calculated trajectory heights.

As indicated earlier, it is well known that pollution from coal-fired power stations in South Africa are characterised by coincidental increases in SO_2, NO_2 and NO (Collet *et al.,* 2010; Lourens *et al.,* 2011; Belaid *et al.,* 2014; Pretorius *et al.,* 2015). However, according to Shirai *et al.* (2012), it is possible for H_2S to be formed during coal-fired power generation if low-NO_x combustion principles are applied. Several papers have been published that indicate that ESKOM have indeed been switching to low-NOx burners in order to move closer to compliance with more stringent NOx emission standards (e.g. Van der Merwe *et al*., 2017; Engineering News, 2017). Another reason for the presence of H_2S could be that a non-ideal oxidative environment is experienced when a coal-fired boiler is started up, which could lead to some H_2S also being emitted. Typically, a cold boiler is initially started by injecting fuel oil at a high pressure through nozzles (ESKOM, 2019), which does not represent boiler conditions at full load and temperature (approximately 1200°C) (ESKOM, 2019). Since 2007, South Africa has been in an energy crisis due to an increase in electricity demand and poor maintenance of the coal-fired power stations (Pretorius *et al.,* 2015). These factors have resulted in more than normal breakdowns (and associated start-ups) of coal-fired power station boilers.

4.4.4 Case study for an urban plume

The term “urban” within the context of this study refers to any measured plume associated with a town/city/informal or semiformal settlement, which include sources such as waste water treatment facilities, landfills, household combustion emissions, small industries and vehicle emissions (especially from older diesel engines). However, plumes from the Jhb-Pta megacity were not included in this source type, since they were considered separately. Figure 4.16 presents a Google Earth image of the small town Bethal (approximately 25km from Elandsfontein) and its associated settlements.

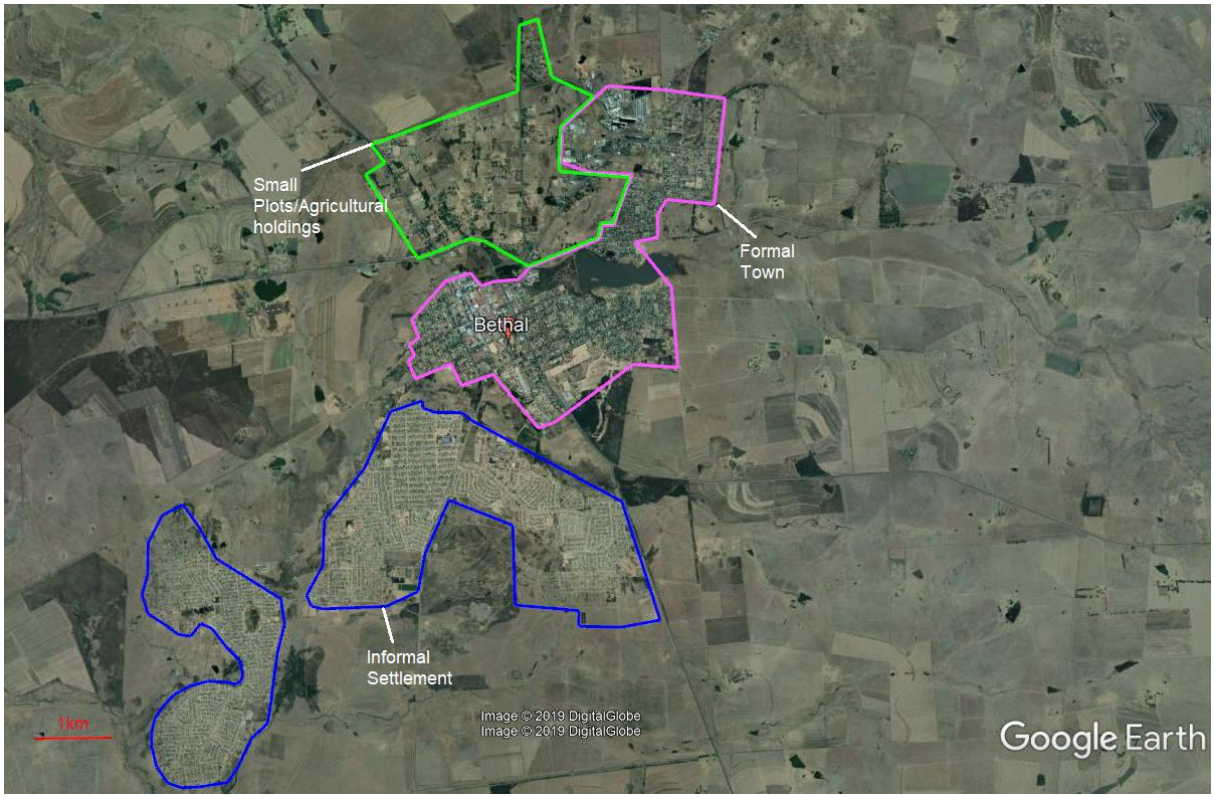

Figure 4.16: Google Earth image of the small town of Bethal. The red line represents 1 km (for scaling purposes). The purple polygon indicates the formal residential area of Bethal, the blue polygons the semi- and informal settlements associated with Bethal, and the green polygon small agricultural plots/holdings.

In Figure 4.17, an increase in H_2S, SO_2 and NO_2 is observed, together with a small increase in eBC, but no increase in NO, between 01:00 and 05:00 on the 19th of February 2009. As proved by previous authors, a peak with coincidental increase of these species is indicative of household combustions on the Mpumalanga Highveld (Chiloane *et al.,* 2017). The combustion processes applied during these practises (especially in informal and semiformal settlements) are not effective enough to oxidise all the sulphur (S) in the fuel to SO_2, therefore H_2S is also emitted. Low quality coal is mostly used as fuel on the Mpumalanga Highveld due to the availability and cheap cost thereof in this region (Balmer, 2007). NO is mostly absent from these plumes, since the PBL is usually very stable (ineffective mixing), especially during the evenings and early mornings of the colder months, leading to significant oxidation of NO to NO_2 before the air mass starts to move.

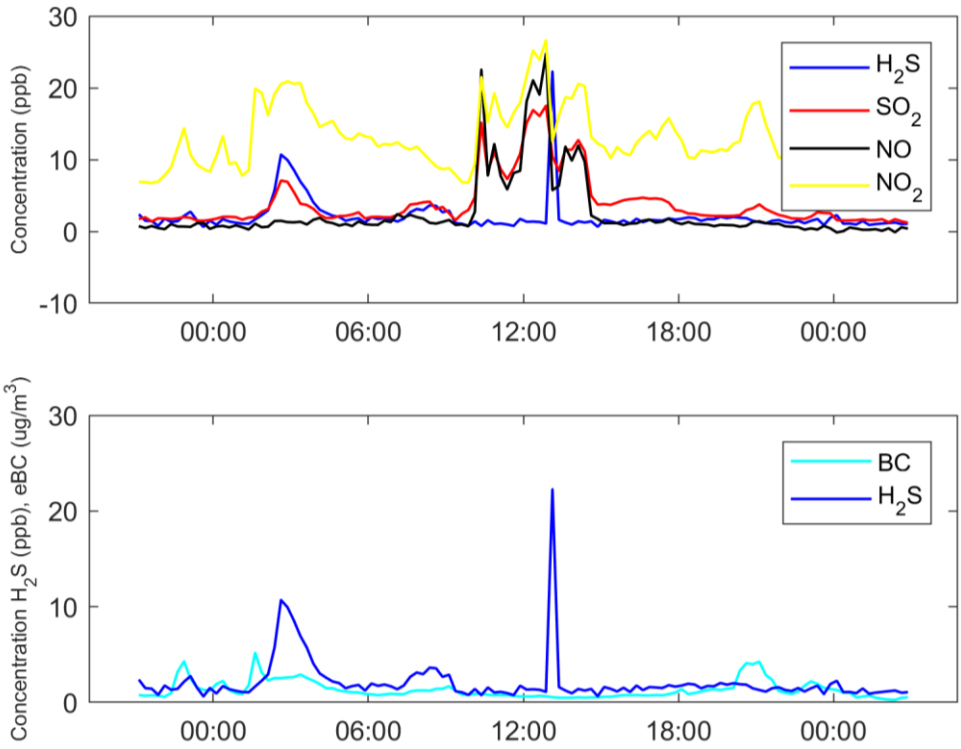

Figure 4.17: 24hr ± 3hr concentration vs. time graphs of co-incidental increases of H_2S, SO_2, NO_2 and eBC on the 19th of February 2009.

The timing of the co-incidental concentration peaks rules out high stack emission (e.g. from coal-fired power stations or the petrochemical operation near Secunda) as a possible source, as it will only be measured when the thermal inversion layer breaks up in the morning and the depth of the PBL increases, which will allow downward mixing of such emissions (Garstang *et al*., 1996; Korhonen *et al*., 2014; Gierens *et al*., 2019). Thus, these emissions were most likely emitted at ground level or beneath the stable nocturnal PBL. This is supported by the calculated trajectory heights presented in Figure 4.18a, which depicts the heights of each calculated back trajectory during the measured plume period. However, from the horizontal back trajectory paths (Figure 4.18b), it is evident that the air mass had passed over two urban settlements. Considering all the aforementioned, this morning plume originated from household combustion and was therefore categorised as an urban emission.

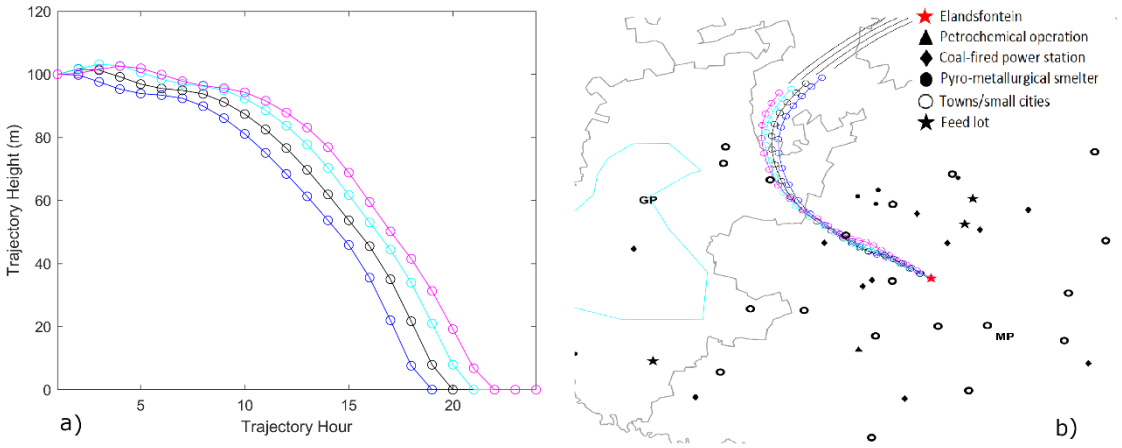

Figure 4.18: a) Calculated vertical back trajectory heights. b) Horizontal back trajectory paths arriving on the hour for the identified plume in Figure 4.17, corresponding to the calculated trajectory heights.

4.4.5 Case study for the Jhb-Pta megacity

The Jhb-Pta megacity is a large conurbation (more than 10 million inhabitants, Lourens *et al*., 2012 and 2016) with a diverse mixture of potential H_2S sources. Being such a large area source, it was categorised separately from the other urban emissions in this study. In Figure 4.19, co-incidental increases in H_2S, SO_2 and NO_2, but no NO, were observed between 04:00 and 10:00 on the 19th of May 2009. The reason for the coincidental increase in the aforementioned species and absence of NO is similar to that discussed for the urban emission in Par. 4.5.4. In addition, the Jhb-Pta area is also further from the measurement site than some of the smaller towns/cities/settlements, which allowed even more time for oxidation of NO to NO_2.

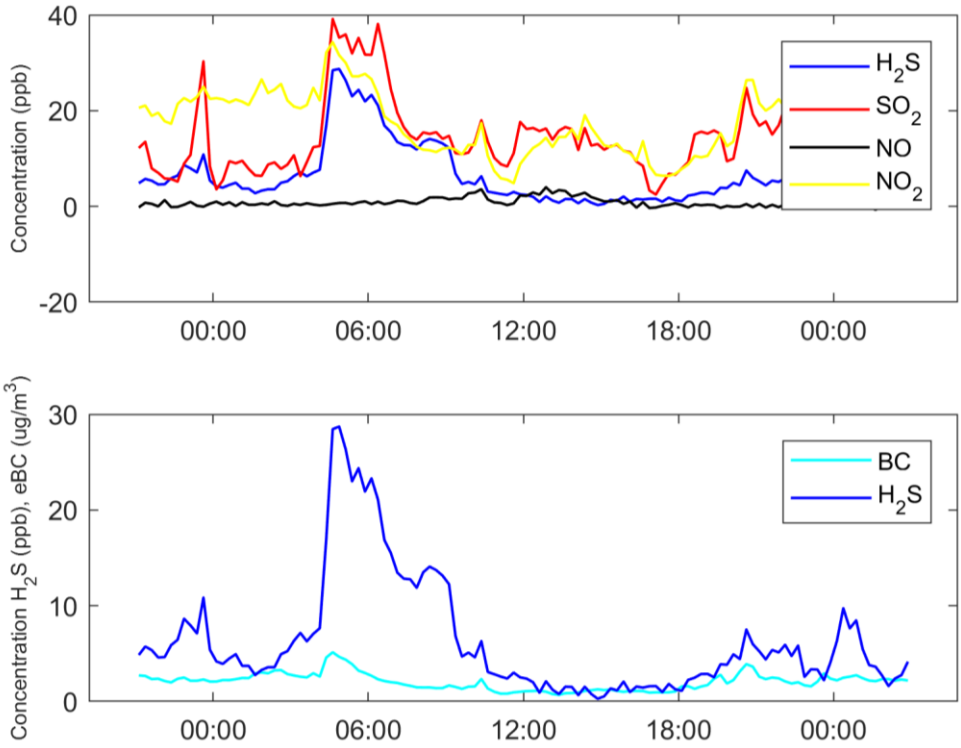

Figure 4.19: 24hr ± 3hr concentration vs. time graphs of co-incidental increases of H_2S, SO_2, NO_2 and eBC between 04:00 and 10:00 on the 19th of May 2009.

As with previous discussions, the timing of the selected co-incidental concentration peaks suggests low-level emissions (Stull, 1988; Korhonen *et al.,* 2014; Gierens *et al.,* 2018) to be the origin. This is further verified by the calculated back trajectory heights (Figure 4.20a), which indicated that the air masses travelled below 100m above ground level as it passed over the mega city. Furthermore, from the calculated horizontal back trajectory paths (Figure 4.20b), it is obvious that the trajectories passed over the Jhb-Pta conurbation (blue polygon). Considering all the aforementioned, it is evident that the measured plume originated from the Jhb-Pta conurbation.

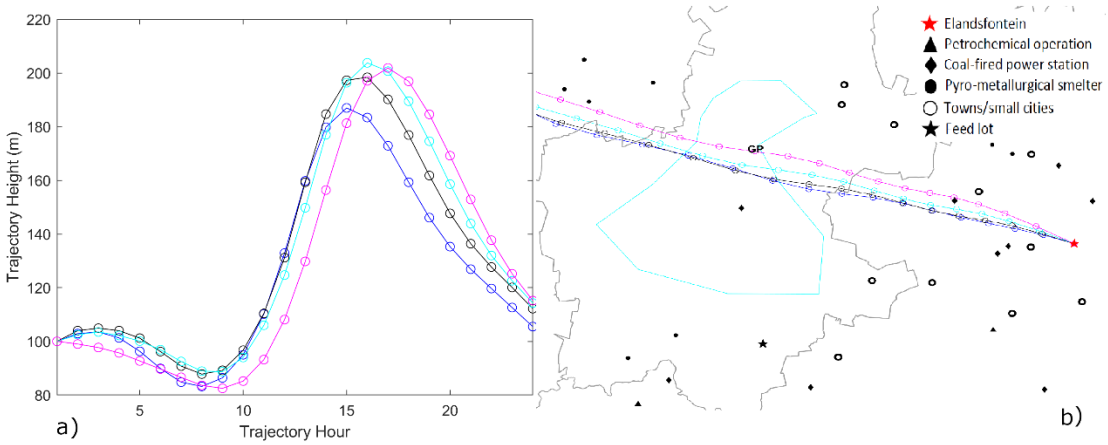

Figure 4.20: a) Calculated vertical back trajectory heights. b) Horizontal back trajectory paths arriving on the hour for the identified plume in Figure 4.19, corresponding to the calculated trajectory heights.

4.4.6 Case study for a cattle feedlot

There are three large cattle feedlots relatively close to the Elandsfontein measurement station. Figure 4.21 presents a Google Earth image of the Kanhym feedlot (25° 53'40 S, 29° 33'31 E). These feedlots emit pollutants beneath the PBL and are characterised by emissions of reduced sulphur compounds such as H_2S, and nitrogen oxides, depending on the type of animals and feed used at the feedlot (Koelsch *et al.,* 2004; Feilberg *et al.,* 2017). The cattle feedlots on the Mpumalanga Highveld are open, dry feedlots, meaning that animals are not kept in confined environments. However, at the Kanhym cattle feedlot (Figure 4.20), there is also a very large piggery. The pigs are housed in closed buildings and also contribute significantly to gaseous emissions.

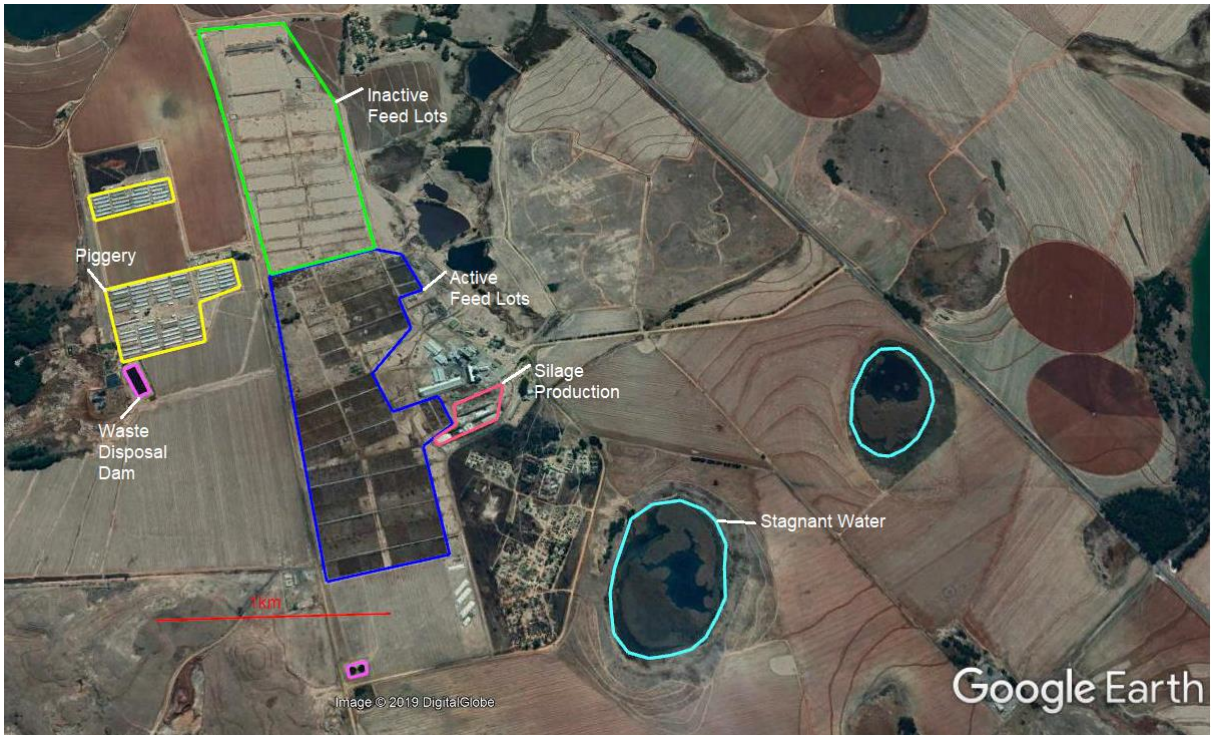

Figure 4.21: Google Earth image of the Kanhym feedlot and piggery. In the image the red line indicates a ruler of 1km (for scaling purposes). The blue polygon indicates active feedlots, the green polygon shows inactive feedlots, the yellow polygons indicate the piggery, purple polygons are waste treatment dams, pink polygons are silage production areas and the cyan polygons indicate stagnant water bodies.

In Figure 4.21, a simultaneous increase of H_2S, SO_2 and NO_2 is observed between 09:00 and 11:00 on the 14th of April 2009. It was not expected to observe an increase in SO_2 in a feedlot plume, but this could be due to fractional oxidation of emitted H_2S to SO_2 during transport of the air mass. The northern interior of South Africa is in general characterise by relatively high O_3 concentrations (e.g. Laban *et al.*, 2018). Although not yet measured in the South African interior, high O_3 will also lead to associated high hydroxyl radical ($OH^{\bullet}$) concentrations (Seinfield & Pandis, 2006). These two species are some of the most important atmospheric oxidants (Seinfield & Pandis, 2006). Additionally, co-

emission of SO_2 from combustion sources at the feedlot (e.g. heavy vehicles, refuse combustion and household combustion) could also have contributed to it being measured as a co-incidental species.

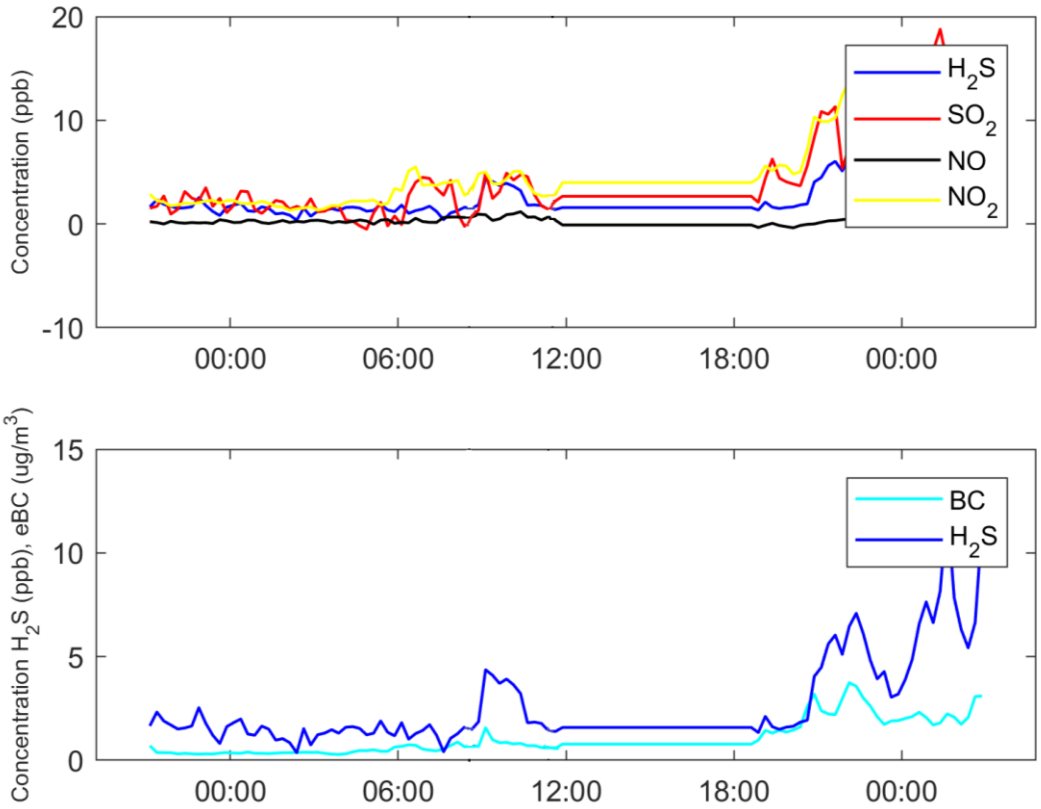

Figure 4.22: 24hr ± 3hr concentration vs. time graphs of co-incidental increases of H_2S, SO_2 and NO_2 on the 14th of April 2009.

The timing of the co-incidental concentration peaks does not eliminate high stack emission as a potential source, since it was observed after the breakup of low-level thermal inversion layers and growth of the PBL typically start (Garstang *et al*., 1996; Korhonen *et al*., 2014; Gierens *et al*., 2019). However, the calculated trajectory heights and vertical back trajectory paths presented in Figures 4.22 (a & b) clearly prove that the air masses had passed at the appropriate height over the Kanhym feedlot and close to the SIS feedlot. Although one of the back trajectories passed close to a coal-fired power station, the peak amplitudes were not indicative of the power station as a source and the air mass travelled very close to ground level at that time. Considering all the aforementioned, this plume was associated with feedlot emissions.

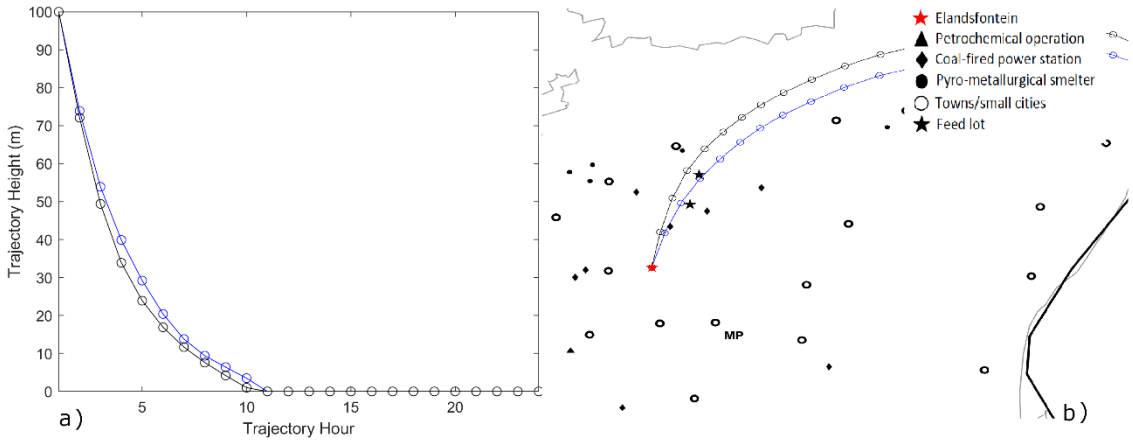

Figure 4.23: a) Calculated vertical back trajectory heights. b) Horizontal back trajectory paths arriving on the hour for the identified plume in Figure 4.22, corresponding to the calculated trajectory heights.

4.5 H_2S source apportionment

Figure 4.22 is a simple bar plot presenting the results of the H_2S receptor source apportionment conducted with the novel method described in Par. 4.3. Co-incidental concentration peaks were allocated, as explained in Par. 4.4., to eight different sources. These were the petrochemical operation near Secunda (indicated as “Petrochemical”), mixed petrochemical near Secunda (indicated as “Mixed petrochemical”), coal-fired power stations (indicated as “Power”), pyrometallurgical smelters (indicated as “Pyrometallurgical”), urban, Jhb-Pta, feedlots and mixed no petrochemical near Secunda (indicated as “Mixed no petrochemical”). The names of these sources are self-explanatory, except the “Mixed petrochemical” and “Mixed no petrochemical”, which require brief clarification. Co-incidental concentration peaks that were a mixture of emissions from the petrochemical operation near Secunda and other source(s) were classified as “Mixed petrochemical”. In contrast, the term “Mixed no petrochemical” refers to co-incidental concentration peaks that were attributed to more than one source but did not include the petrochemical operation near Secunda.

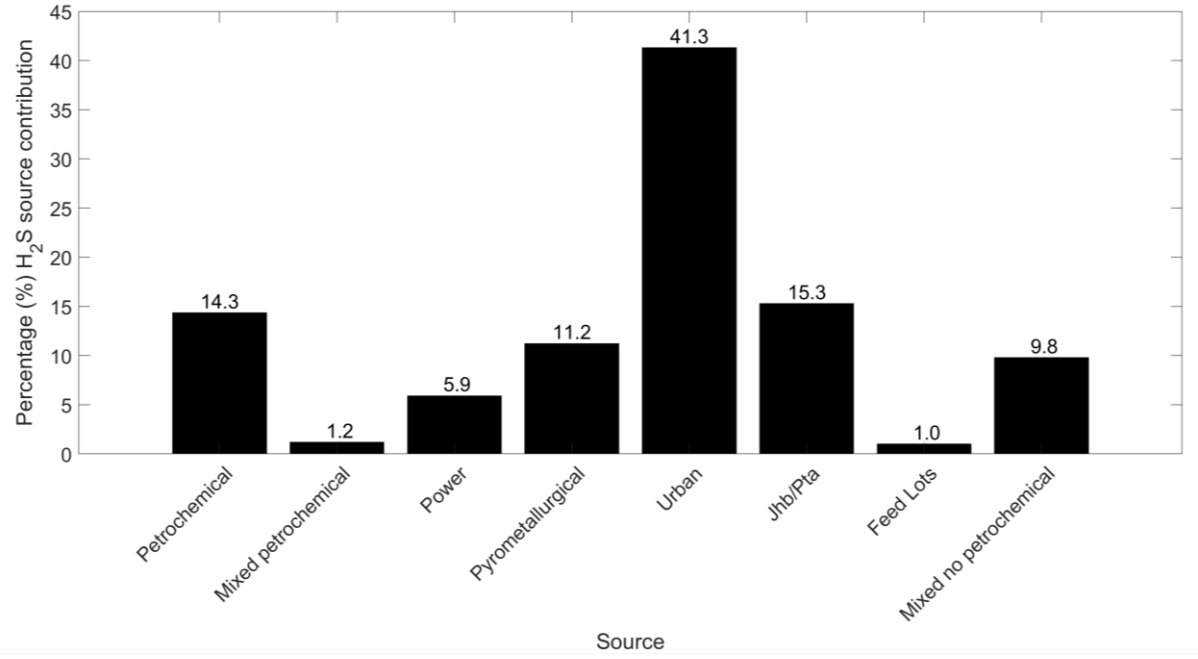

Figure 4.24: Percentage source contribution of each of the identified sources as calculated by the novel source apportionment method discussed in Section 4.2.

It is evident from Figure 4.24 that the main contributors to ambient H_2S measured in excess of the baseline concentrations typically observed at Elandsfontein, were from urban emissions (i.e. approximately 41.3%). As previously stated, these urban emissions include all H_2S emissions associated with cities/towns/in- and semiformal settlements (but exclude emissions from the Jhb-Pta megacity) such as household combustion, waste water treatment facilities, landfills, small industries and traffic emissions, especially from older diesel vehicles (Kourtidis *et al.,* 2004; Sengupta, 2014; Colomer *et al.,* 2015; Hac Ko *et al.,* 2015). In Figure 4.2 (Par. 4.2), i.e. the diurnal H_2S patterns, bimodal peaks were identified in the early mornings and evenings and were attributed to low-level emissions that can be trapped near the surface layer by inversions and the shallow PBL (Garstang *et al*., 1996; Korhonen *et al*., 2014; Gierens *et al*., 2019). Therefore, the afore-mentioned results, i.e. that urban emissions are the main contributor to H_2S measured at Elandsfontein, correlate with the deductions made from the diurnal patterns.

The Jhb-Pta conurbation was found to be the second largest contributor to H_2S measured in excess of the baseline concentrations typically observe at Elandsfontein, with approximately 15.3% (Figure 4.24). Combined, the urban- and Jhb-Pta sources accounted for approximately 56.6% of the H_2S in excess of the baseline.

It is well known that the petrochemical operation near Secunda emits H_2S since the pyrolysis coal gasification process applied (Bunt & Waanders, 2008) suppress the formation of oxidised gas species. However, from the receptor source apportionment results it is evident that it is not the main

contributor of H_2S measured at Elandsfontein, since it contributed approximately 14.3% of the H_2S measured in excess of the baseline concentrations (Figure 4.24). Even if the "Mixed petrochemical" contribution of approximately 1.2% is added to this, its overall maximum contribution does not significantly increase.

In a previous study done by Chiloane *et al.* (2017), it was found that the pyrometallurgical smelters in the Middelburg/Witbank area contributed to H_2S measured at Elandsfontein on the Mpumalanga Highveld, however, its factional contribution was unknown. The current results (Figure 4.24) indicated that the pyrometallurgical smelters in the area contributed approximately 11.2% of H_2S measured in excess of the baseline concentrations at Elandsfontein.

The coal-fired power stations also contributed to the ambient H_2S measured in excess of the baseline concentrations at Elandsfontein, with a smaller, but not insignificant contribution of approximately 5.9% (Figure 4.24). As indicated earlier (Par. 4.4.3), this was an unexpected result. However, two possible reasons for emission of H_2S from coal-fired power stations could be established, i.e. use of low-NO_x burners (Shirai *et al.,* 2012; Van der Merwe *et al*., 2017; Engineering News, 2017) and non-ideal oxidative environment experienced during boiler start-ups (ESKOM, 2019).

Feedlots had the smallest individual contribution to the ambient H_2S measured in excess of baseline concentrations at Elandsfontein (approximately 1.0%). Three very large feedlots, each with ≥ 10 000 cattle, could be identified as sources. These animals do not directly emit H_2S, but there are generally two sources at feedlots where H_2S is produced (Sakirkin *et al*., 2012): i) in waste runoff retention structures or treatment lagoons and ii) accumulation of manure in pens and manure storage areas (Sakirkin *et al.,* 2012). In both of these locations, anaerobic wet conditions allow for the decomposition of manure to produce H_2S (Sakirkin *et al.,* 2012; Rubright *et al.,* 2017). Additionally, anaerobic decomposition of silage feed could also serve as a small H_2S source, but, as far as the candidate could determine, no studies have been conducted to assess this potential source. It is generally accepted that feedlots do not emit H_2S in very large quantities (Koelsch *et al., 2004*), therefore the results (Figure 4.24) make sense.

Lastly, the co-incidental concentration peaks that were attributed to "Mixed no petrochemical" sources contributed approximately 9.8% of the H_2S measured in excess of the baseline concentrations at Elandsfontein. Apart from emissions originating from a mixture of sources that could not be separated from one another with the method presented in this study, this source group also includes emissions from burning coal dumps on the Mpumalanga Highveld (Schoeman, 2016), which could be a potentially significant source of H_2S.

4.6 Conclusion of results and discussion

The novel method developed in this study (Par. 4.3) was successfully used to conduct the first receptor source apportionment of ambient H_2S in excess of the baseline concentrations measured at Elandsfontein on the Mpumalanga Highveld (Par. 4.5). Emissions from urban areas (excluding the Jhb-Pta conurbation) were identified as the largest source contributor, which accounted for approximately 41.3% of the emitted H_2S. In addition, the Jhb-Pta megacity contributed another 15.3%, which was similar to the contribution from the petrochemical operation near Secunda (approximately 14.3%, and possibly 1.2% additionally from mixed sources that included the petrochemical operation near Secunda). Pyrometallurgical operations, coal-fired power stations and large feedlots contributed approximately 11.2, 5.9 and 1.0%, respectively. Mixed sources which did not include any contribution from the petrochemical operation near Secunda accounted for 9.8% of the contributed H_2S. 11% of H_2S could not be allocated to a specific source using the novel receptor source apportionment method. However, 89% of ambient H_2S measured in excess of the baseline was successfully attributed to a specific source.

The source appointment results also correlated well with the deductions made from the temporal assessments (Par. 4.2). Higher ambient H_2S concentrations were observed in the colder months. Additionally, bimodal peaks (the early morning and evening), as well as a peak after the breakup of the low-level thermal inversion(s) and growth of the PBL depth (Garstang *et al*., 1996; Korhonen *et al*., 2014; Gierens *et al*., 2019), were observed in the diurnal cycles. These results indicate that low-level emission sources were the main contributor to ambient H_2S measured at Elandsfontein, with high stack emission also being an important (but not dominant) source.

Chapter 5: Conclusions, project evaluation and future perspectives

In this chapter, the main conclusions are reconsidered in Par. 5.1, where after the project is evaluated in Par. 5.2 against the objectives that were set in Chapter 1. Lastly, future perspectives are discussed in Par. 5.3.

5.1 Conclusions

In this study the first receptor-oriented source apportionment for hydrogen sulphide (H_2S) on the Mpumalanga Highveld is presented. A novel receptor source apportionment technique was developed, based on the method published by Chiloane *et al*. (2017), to conduct this source apportionment study. Existing receptor source apportionment techniques were not suited for trace gas source apportionment and source-oriented models were not considered, as a comprehensive peer reviewed South African specific emission inventory was not available in the public domain at the time when this study commenced. The main deductions from the study are subsequently considered.

- The data availability of 75% after data cleaning and data quality/assurance procedures had been applied, was sufficient to enable receptor source apportionment. Most of the data gaps were due to power outages, while removal of bad/suspicious data also contributed. The data gaps were spread throughout the data set, therefore avoiding temporal bias (Par. 3.3, Par. 4.1).
- From the contextualisation of the mean/median H_2S concentrations observed at Elandsfontein, it was evident that this site is relatively polluted and that H_2S levels were comparable to mean/median values reported for suburbs near gas processing plants in Arkansas (USA), or curbside measurements in Thessaloniki (Greece). However, the H_2S levels at Elandsfontein were not as high as at the heavily polluted Rotorua in New Zealand (Par. 4.1).
- From temporal H_2S patterns (monthly and diurnal), it was deduced that low-level emissions of H_2S likely dominate ambient concentrations at Elandsfontein, but that high stack emissions also made a significant contribution. However, from these temporal patterns it was impossible to identify specific sources (Par. 4.2).
- A novel source apportionment technique, based on the method described by Chiloane et al. (2017), was developed (Par. 4.3). The technique was modified by combining all seperate processes of the method into one coherent semi-automated method/program, and additionally smaller sources (e.g. towns/cities, feedlots, etc.) were also considered. It was proven that, by considering co-incidental increases in trace gas and equivalent black carbon (eBC) ambient concentrations measured at Elandsfontein, different sources of H_2S could be identified due to their unique emission profiles, time of measurement (due to thermal

inversions and the planetary boundary layer structure preventing vertical mixing at certain times), as well as concentration peak duration and amplitude (which helped differentiate large point and area sources from one another). By considering back trajectories calculated during the observed co-incidental peak, the horizontal paths could be used to confirm that the air masses had passed over/close to a specific source(s), while the trajectory heights could be used to confirm emission heights (Pars. 4.3-4.4).

- The source apportionment results indicated that the main contributor to ambient H_2S measured at Elandsfontein is urban emissions (towns, as well as semi- and informal settlements, waste water treatment facilities, landfills, small industries and traffic), which excluded emissions from the Johannesburg-Pretoria (Jhb-Pta) conurbation. These urban emissions contributed 41.3% in excess of the baseline H_2S concentrations. The Jhb-Pta conurbation was classified as a separate source due to its size. It contributed second most to ambient H_2S in excess of the baseline, with 15.3%. Combined, the urban and Jhb-Pta sources contributed 56.6% of the ambient H_2S in excess of the baseline. The petrochemical operation near Secunda was found to contribute 14.3% to the ambient H_2S in excess of the baseline concentrations. Furthermore, pyrometallurgical smelters, coal-fired power stations and cattle feedlots contributed 11.2, 5.9 and 1.0% to the ambient H_2S in excess of the baseline, respectively. In the study, 11% of ambient H_2S could not be allocated to specific sources. Therefore, 89% of ambient H_2S measured at Elandsfontein in excess of the baseline was apportioned successfully.

5.2 Project evaluation

In order to evaluate the project, each of the stated objectives (Par. 1.2) are reconsidered in context of the successes and/or shortcomings in achieving it.

Objective 1: Modify and further develop the existing source apportionment method presented by Chiloane *et al.* (2017) to enable source apportionment of trace gases.

From the results (Chapter 4), it is evident that the modified technique is suitable for receptor-oriented source apportionment of trace gas species. Therefore, the model was successfully developed further. However, it will not be possible to use this receptor modelling technique on all datasets, since a comprehensive data set (with many simultaneous measured species) of active measurement (highly time resolved measurements) is needed. As with all receptor models, the technique also requires significant source knowledge as user input.

Objective 2: Identify unique characteristics, e.g. co-incidental concentration peaks, plume times, duration and amplitude, and air mass movements, to isolate different H_2S sources.

Specific sources of H_2S were identified with the novel technique by retrieving information from the co-incidental concentration peaks, plume times, duration and amplitude, and air mass movements. The sources were identified as urban emissions, the Jhb-Pta conurbation, the petrochemical operation near Secunda, pyrometallurgical smelters, coal-fired power stations, and cattle feedlots. In Par. 4.4, different case studies were presented on how the specific sources were differentiated. Burning coal dumps could not be isolated as a separate source, although they are highly likely to be important emission contributors on the Mpumalanga Highveld.

Objective 3: Conduct source apportionment of H_2S measured at Elandsfontein.

Source apportionment of ambient H_2S measured at Elandsfontein was done successfully, with 89% of the H_2S measured in excess of the baseline being attributed to sources. The remaining 11%, which could not be attributed, can possibly be reduced further if burning coal dump emissions can be isolated.

5.3 Future perspectives

Although the objectives were successfully achieved and deeper understanding with regard to H_2S source apportionment on the Mpumalanga Highveld was gained, the new insights also brought about new/additional questions pertaining to the topic. In essence, this is what scientific research should do, i.e. answer questions and raise new questions in order to achieve continued improvement. According to the candidate, at least four topics should be addressed in future investigations.

- As indicated earlier, it is necessary to include burning coal dumps as a source of H_2S at Elandsfontein. To do so, it will be necessary to determine the temporal burning activities of coal dumps (when did these dumps burn?) on the Mpumalanga Highveld. This could possibly be achieved by applying the method relatively recently published by Beukes *et al*. (2018), wherein radiative power data, measured with satellite instruments, are used to derive activity patterns of emission sources associated with thermal emissions.
- In the current study, only co-incidental peaks in excess of the H_2S baseline concentrations were considered. The total time of all such peaks added up to approximately 20% of the overall time of the dataset. Therefore, there is still a significant amount of H_2S unaccounted for (not attributed to a source), which is likely emitted by small/defuse H_2S sources (e.g. decomposition of animal and plant matter, stagnant water bodies, low population density areas). It is important to quantify this baseline/background H_2S, since it is vital to understand the baseline/background H_2S levels before regulation of larger sources are considered.

- This study established that the developed method is effective in doing source apportionment of trace gas species (although it was only applied for H_2S as measured at Elandsfontein). Therefore, in future, similar source apportionment of the other sulphur-, as well as nitrogen-containing trace gas species (nitrogen oxide, nitrogen dioxide and sulphur dioxide) should be done for Elandsfontein. This will enable total sulphur and nitrogen source apportionment, which is very important within impact study perspectives (e.g. Conradie *et al*., 2016).
- Currently, the developed method is semi-automated. Further development (e.g. with computer learning and other automation techniques) should strive to automate the method further to enable a wider user community (which might not be so well versed in regional source knowledge).

Bibliography

ABDI, H., WILLIAMS, L.J. 2010. Principal component analysis. *Interdisciplinary Reviews Computational Statistics*. 2 (4), 733-459, doi: https://doi.org/10.1002/wics.101.

ABDUL-WAHAB, S.A., BAKHEIT, C.S., AL-ALAWI, S.M. 2005. Principal component and multiple regression analysis in modelling of ground-level ozone and factors affecting its concentrations. *Environmental Modelling & Software*, 20 (10), 1263–1271, doi: 10.1016/j.envsoft.2004.09.001.

AIRSHED PLANNING PROFESSIONALS. 2017. Atmospheric Impact Report: Sasol Secunda Synfuels Operations. Report no.: 16SAS03, Rev 1.

AIR RESOURCES LABORATORY. 2014. National Oceanic and Atmospheric Administration (NOAA). http://www.arl.noaa.gov/ Date of access: 20 Jul. 2019.

ATKINSON, R. 2000. Atmospheric chemistry of VOCs and NOx. *Atmospheric Environment,* 34(12–14):2063–2101.

BAARS, H., KANITZ, T., ENGELMANN, R., ALTHAUSEN, D., HEESE, B., KOMPPULA, M., PREIßLER, J., TESCHE, M., ANSMANN, A., WANDINGER, U., JAE-HYUN L., JOON YOUNG A., STACHLEWSKA, I.S., AMIRIDIS, V., MARINOU, E., SEIFERT, P., HOFER, J., SKUPIN, A., SCHNEIDER, F., BOHLMANN, S. 2016. An overview of the first decade of PollyNET: an emerging network of automated Raman-polarization lidars for continuous aerosol profiling. *Atmospheric Chemistry & Physics*, 16, 5111–5137, doi: 10.5194/acp-16-5111-2016.

BACKMAN, J., VIRKKULA, A., VAKKARI, V., BEUKES, J.P., VAN ZYL, P.G., JOSIPOVIC, M., PIKETH, S., TIITTA, P., CHILOANE, K., PETÄJÄ, T., KULMALA, M., LAAKSO, L. 2014. Differences in aerosol absorption Angstrom exponents between correction algorithms for a particle soot absorption photometer measured on the South African Highveld. *Atmospheric Measurement Techniques*, 7, 4285-4298, doi: https://doi.org/10.5194/amt-7-4285-2014.

BALMER, M. 2007. Household coal use in an urban township in South Africa. *Journal of Energy in Southern Africa*, 18, 27-32, doi: http://dx.doi.org/10.17159/2413-3051/2007/v18i3a3382.

BELAID, M., FALCON, R., VAINIKKA, P. 2014. Pulverized coal versus circulating fluidized-bed boilers Perspectives and challenges for South Africa. *South African Journal of Chemical Engineering*, 19, 72-81.

BELIS, C.A., LARSON, B.R., AMATO, F., EL HADDAD, I., FAVEZ, O., HARRISON, R.M., HOPKE, P.K., NAVA, S., PAATERO, P., QUASS, U., VECCHI, R., VIANA, M., PREVOT, A. 2014. European Guide on Air Pollution Source Apportionment with Receptor Models; Joint Research Centre, Institute for Environment and Sustainability: Luxembourg: Publications Office of the European Union, doi: 10.2788/9307.

BEUKES, J.P., VENTER, A.D., JOSIPOVIC, M., VAN ZYL, P.G., VAKKARI, V., JAARS, K., DUNN, M. & LAAKSO, L. 2015. Automated continuous air monitoring. (*In* FORBES, P., *ed*. Monitoring of Air Pollutants – Sampling, Sample, Preparation and Analytical Techniques, Elsevier. In press.).

BEUKES, J.P., DU PREEZ, S.P., VAN ZYL, P.G., PAKTUNC, D., FABRITUS, T., PÄÄTALO, M., CRAMER, M. 2017. Review of Cr(VI) environmental practices in the chromite mining and smelting industry – Relevance to development of the Ring of Fire, Canada. Journal of Cleaner Production, 165, 874-889, doi: http://dx.doi.org/10.1016/j.jclepro.2017.07.176.

BEUKES, J.P., VAN ZYL, P.G., SIFIEV, M., SOARES, J., LIEBENBERG-ENSLIN, H., SHACKLETON, N., SUNSTRÖM, A.-M. 2018. The use of satellite observations of fire radiative power to estimate the availabilities (activity patterns) of pyrometallurgical smelters. *The Journal of the Southern African*

Institute of Mining and Metallurgy, 118, 619-624, doi: http://dx.doi.org/10.17159/2411-9717/2018/v118n6a9.

BHAVE, P.V., FERGENSON, D.P., PRATHER, K.A., CASS, G.R. 2001. Source apportionment of fine particulate matter by clustering single-particle data: Tests of receptor model accuracy. *Environmental Science and Technology*, 35, 2060-2072. doi:10.1021/es0017413.

BRUWER, A.P., KORNELIUS, G. 2017. Modeling the effects of biogenic NOx emissions on the South African Highveld and Waterberg regions. *Water, Air & Soil Pollution*, 228:326, doi: https://doi.org/10.1007/s11270-017-3526-y.

BUNT, J.R., WAANDERS, F.B. 2008. Identification of the reaction zones occurring in a commercial-scale Sasol-Lurgi FBDB gasifier. *Fuel*, 87, 1814-1823, doi: 10.1016/j.fuel.2007.11.012.

CAMACHO, A. 2009. Sulphur Bacteria. (*In* LIKENS, G.E., Plankton of Inland Waters, 1st Edition), 261-279 p.

CARDOSO, A.A., LIU, H., DASGUPTA, P.K. 1996. Fluorometric fiber optic drop sensor for atmospheric hydrogen sulphide. *Talanta*, 44:1099–1106, doi: https://doi.org/10.1016/S0039-9140(96)02202-3.

CHILOANE, K.E., BEUKES, J.P., VAN ZYL, P.G., MARITZ, P., VAKKARI, V., JOSIPOVIC, M., VENTER, A.D., JAARS, K., TIITTA, P., KULMALA, M., WIEDENSOHLER, A., LIOUSSE, C., MKHATSHWA, G.V., RAMANDH, A., LAAKSO, L. 2017, Spatial, temporal and source contribution assessments of black carbon over the northern interior of South Africa. *Atmospheric Chemistry & Physics,* 17,6177-6196, doi: 10.5194/acp-17-6177-2017.

CHOU, S., OGDEN, J.M., PHOL, H.R., SCINICARIELLO, F., INGERMAN, L., BARBER, L., CITRA, M. 2016. Toxicalogical profile for hydrogen sulphide and carbonyl sulphide. Agency for Toxic Substances and Disease Registry: Atlanta, GA.

CONRADIE, E.H., VAN ZYL, P.G., PIENAAR, J.J., BEUKES, J.P., GALY-LACAUX, C., VENTER, A.D., MKHATSHWA, G.V. 2016. The chemical composition and fluxes of atmospheric wet deposition at four sites in South Africa. *Atmospheric Environment*, 146, 113-131, doi: http://dx.doi.org/10.1016/j.atmosenv.2016.07.033.

COLLETT, K.S., PIKETH, S.J., ROSS, K.E. 2010. An assessment of the atmospheric nitrogen budget on the South African Highveld. *South African Journal of Science*, 106(5/6), Art. #220, 9 pages, doi: 10.4102/sajs.v106i5/6.220.

COLOMER, F.L., MORATÓ, H.E., IGLESIAS, E.M. 2012. Estimation of hydrogen sulfide emission rates at several wastewater treatment plants through experimental concentration measurements and dispersion modelling. *Journal of the Air & Waste Management Association*, 62:7, 758-766, DOI: 10.1080/10962247.2012.674008.

CONTINI, D., CESARI, D., CONTE, M., DONATEO, A. 2016. Application of PMF and CMB receptor models for the evaluation of the contribution of a large coal-fired power plant to PM_{10} concentrations. *Science of the Total Environment*, 560-561, 131-140, doi: http://dx.doi.org/10.1016/j.scitotenv.2016.04.031.

COOPER, J.A., WATSON, JR. J.G. 1980. Receptor Oriented Methods of Air Particulate Source Apportionment. *Journal of the Air Pollution Control Association,* 30:10, 1116-1125, doi: 10.1080/00022470.1980.10465157.

DABROWSKI, J.M., ASHTON, P.J., MURRAY, K., LEANER, J.J., MASON, R.P. 2008. Anthropogenic mercury emissions in South Africa: Coal combustion in power plants. *Atmospheric Environment*, 42(27):6620–6626.

DALY, A., ZANNETTI, P. 2007. An Introduction of Air Pollution - Definitions, Classifications, and History. (*In* ZANNETTI, P., AL-AJMI, D. & AL-RASHIED, S., *eds*. Ambient air Pollution, The Arab School for Science and Tegnology (ASST) and The EnviroComp Institue. 1-14 p.)

DELMAS, R., BAUDET, J., SERVANT, J., BAZIARD, Y. 1980. Emissions and concentrations of hydrogen sulfide in the air of the tropical forest of the Ivory Coast and of temperate regions in France. *Journal of Geophysical Research*, 85, 148-227, doi: 10.1029/JC085iC08p04468.

DEPARTMENT OF ENVIRONMENTAL AFFAIRS. 2007, Government Gazette, 23 November, No. 30518.

DEPARTMENT OF ENVIRONMENTAL AFFAIRS. 2009, Government Gazette, 24 December, No. 32816.

DEPARTMENT OF ENVIRONMENTAL AFFAIRS. 2009, State of Air Report 2005. A report on the state of air in South Africa.

DEPARTMENT OF ENVIRONMENTAL AFFAIRS. 2010, The Highveld Priority Area Air Quality Baseline Assessment Report 2010.

DORAISWAMY, P., DAVIS, W.T., MILLER, T.L., FU, J.S. 1995. Source apportionment of fine particles in Tennessee using a source-oriented model. *Journal of the Air & Waste Management Association,* 57:407-419, doi: 10.3155/1047-3289.57.4.407.

DRAXLER, R.R, HESS, G.D. 2004, Description of the HYSPLIT 4 Modelling System. NOAA Technical Memorandum ERL ARL-224.

DU PREEZ, S.P., BEUKES, J.P., VAN ZYL, P.G. 2015. Cr(VI) Generation During Flaring of CO-Rich Off-Gas from Closed Ferrochromium Submerged Arc Furnaces. *Metallurgical and Materials Transactions*, 46B, 1002-1010, doi: 10.1007/s11663-014-0244-3.

ELDERING, A., CASS, G.R. 1996. Source-orientated model for air pollution effects on visibility. *Journal of Geophysical Research*, 101, (D14). doi: 10.1029/95JD02928.

ENGELBRECHT, J.P., SWANEPOEL, L., CHOW, J.C., WATSON, J.G., EGAMI, R.T. 2002, The comparison of source contributions from residential coal and low-smoke fuels, using CMB modelling in South Africa. *Environmental Science & Policy*. 5:157–167, doi: http://dx.doi. org/10.1016/S1462-9011(02)00029-1.

ENGINEERING NEWS. 2017. Camden power station to receive last of 164 burners. http://www.engineeringnews.co.za/article/camden-power-station-to-receive-last-of-164-burners-2017-01-27. Date of access [18 Feb 2019].

ENVIRONMENTAL PROTECTION AGENCY. “Report to Congress on Hydrogen Sulfide Air Emissions Associated with the Extraction of Oil and Natural Gas.” EPA-453/R-93-045, October 1993.” p.III-4.

ENVIRONMENTAL PROTECTION AGENCY. 2009. Standard Operating Procedures. Thermo Environmental Instruments Model 43C SO_2 analyser. Version no. 2.0.

ENVIRONMENTAL PROTECTION AGENCY. Managing Air Quality – Emissions Inventories. https://www.epa.gov/air-quality-management-process/managing-air-quality-emissions-inventories. Last updated 16 January 2018. Date of access: [23 Jul 2018].

ESKOM. 2019. Power generation overview. www.eskom.co.za/AboutElectricity/FactsFigures/Documents/CO0002HowElecProducedCoalFiredRev11.pdf. Date of access: [22 Feb 2019].

FEILBERG, A., HANSEN, M.J., LIU, D., NYORD, T. 2017. Contribution of livestock H2S to total sulfur emissions in a region with intensive animal production. *Nature Communications*, doi: 10.1038/s41467-017-01016-2.

FENGER, J. 2009. Urban air pollution. (*In* HEWITT, C.N. & JACKSON, A.V., *eds*. Atmospheric Science for Environmental Scientists. Chichester, W. Sussex: Wiley-Blackwell. 242-267 p.)

FREIMAN, M.T., PIKETH, S.J. 2002 Air transport into and out of the industrial Highveld Region of South Africa. *Journal of Applied Meteorology*, 42(7):994–1002, doi: 10.1175/1520-0450(2003)042<0994:ATIAOO>2.0.CO;2.

GARSTANG, M., TYSON, P.D., SWAP, R., EDWARDS, M., KÅLLBERG, P., LINDESAY, J.A. 1996. Horizontal and vertical transport of air over southern Africa. *Journal of Geophysical Research*,101:721–736. http://dx.doi. org/10.1029/95JD00844.

GIANNAKAKI, E., PFÜLLE, A., KORHONEN, K., MIELONEN, T., LAALSO, L., VAKKARI, V., BAARS, H., ENGELMAN, R., BEUKES, J.P., VAN ZYL, P.G., JOSIPOVIC, M., TIITTA, P., CHILOANE, K., PIKETH, S.J., LIHAVAINEN, H., LEHTINEN, K.E.J., KOMPPULA, M. 2015. One year of Ramen lidar observations of free-tropospheric aerosol layers over South Africa. *Atmospheric Chemistry and Physics*, 15, 5429-5442, doi: 10.5194/acp-15-5429-2015.

GIERENS, R.T., HENRIKSSON, S., JOSIPOVIC, M., VAKKARI, V., VAN ZYL, P.G., BEUKES, J.P., WOOD, C.R., O'CONNOR, E.J. 2018. Observing continental boundary-layer structure and evolution over the South African savannah using a ceilometer. *Theoretical Applied Climatology*, doi: 10.1007/s00704-018-2484-7.

GOAR, B.G. 1986. "Sulfur Recovery Technology". *Energy Progress*, 6, 71-75.

HALES, J.M., WILKES, J.O., YORK, J.L. 1974. Some recent measurements of H_2S oxidation rates and their implications to atmospheric chemistry. *Tellus*, 26:1-2, 277-283, doi: 10.3402/tellusa.v26i1-2.9795.

HAC KO, J., XU, Q., JANG, Y.-C. 2015. Emissions and Control of Hydrogen Sulfide at Landfills: A Review. *Critical Reviews in Environmental Science and Technology*, 45:19, 2043-2083, DOI: 10.1080/10643389.2015.1010427.

HENRY, R. C. 1987. Current factor analysis receptor models are ill-posed. *Atmospheric Environment*, *21*, 1815–1820, doi: https://doi.org/10.1016/0004-6981(87)90122-3.

HENRY, R.C. 1991. Multivariate receptor models. *Receptor Modelling for Air Quality Management, Hopke PK (ed*). Elsevier: Amsterdam, 117-147.

HINZ, R. 2011. Hydrogen Sulphide in Rotorua, New Zealand: Personal Exposure Assessment and Health Effects. Palmerston North: Massey University. (Dissertation – M.Sc.) 166p.

HOPKE, P.K. 2008. The use of Source Apportionment for Air Quality Management and Health Assessments. *Journal of Toxicology and Environmental Health*, Part A, 71:9-10, 555-563, doi: 10.1080/15287390801997500.

HOPKE, P.K., COHEN D.D. 2011. Application of receptor modelling methods. *Atmospheric Pollution Research*, 2, 122-125, doi: 10.5094/APR.2011.016.

HOPKE, P.K. 2016. Review of receptor modelling methods for source apportionment. *Jounal of the Air & Waste Management Association*, 66:3, 237-259, doi: 10.1080/10962247.2016.1140693.

HYVäRINEN, A.-P., VAKKARI, V., LAAKSO, L., HOODA, R.K., SHARMA, V.P., PANWAR, T.S., BEUKES, J.P., VAN ZYL, P.G., JOSIPOVIC, M., GARLAND, R.M., ANDREAE, M.O., PÖSCHL, U. & PETZOLD, A. 2013. Correction for a measurement artefact of the Multi-Angle Absorption Photometer (MAAP) at high black carbon mass concentration levels. *Atmospheric Measurement Techniques*, 6:81-90.

INTERGOVERNMENTAL PANEL ON CLIMATE CHANGE. 2013. Climate Change 2013: The Physical Science Basis. *Contribution of Working Group I to the Fifth Assessment Report of the Intergovernmental Panel on Climate Change.* Cambridge University Press, Cambridge, United Kingdom and New York, NY, USA, 1535 pp. http://www.ipcc.ch/report/ar5/wg1/ Date of access: 25 Feb. 2019.

JAARS, K., VAN ZYL, P.G., BEUKES, J.P., HELLÉN, H., VAKKARI, V., JOSIPOVIC, M., VENTER, A.D., RÄSÄNEN, M., KNOETZE, L., CILLIERS, D.P., SIEBERT, S.J., KULMALA, M., RINNE, J., GUENTHER, A., LAAKSO, L., HAKOLA, H. 2016. Measurements of biogenic volatile organic compounds at a grazed savannah grassland agricultural landscape in South Africa. Atmospheric Chemistry and Physics, 16, 15665-15688, doi: 10.5194/acp-16-15665-2016.

JAARS, K., VESTENIUS, M., VAN ZYL, P.G., BEUKES, J.P., HELLÉN, H., VAKKARI, V., VENTER, M., JOSIPOVIC, M., HAKOLA, H. 2018. Receptor modelling and risk assessment of volatile organic compounds measured at a regional background site in South Africa. *Atmospheric Environment*, 172, 133-148, doi: 10.1016/j.atmosenv.2017.10.047.

JAYARATNE, E.R., VERMA, T.S. 2001. The impact of biomass burning on the environmental aerosol concentration in Gaborone, Botswana. *Atmospheric Environment*, 35:1821-1828, doi: 10.1016/S1352-2310(00)00561-6.

KAMPA, M. & CASTANAS, E. 2008. Human heatlh effects of air pollution. *Environmental Pollution*, 151:362-367.

KLEEMAN, M.J., CASS G.R. 2001. A 3D Eulerian Source-Oriented Model for an Externally Mixed Aerosol. *Environmental Science and Technology*, 25, 4834-4848, doi:10.1021/es010886m.

KOELSCH, R.K., WOODBURY, B.L., STENBERG, D.E., MILLER, D.N., SCHULTE, D.D. 2004. Hydrogen Sulfide Concentration in Vicinity of Beef Cattle Feedlots. *Nebraska Beef Cattle Reports*, 198, https://digitalcommons.unl.edu/animalscinbcr/198.

KORHONEN, K., GIANNAKAKI, E., MIELONEN, T., PFULLER, A., LAAKSO, L., VAKKARI, V., BAARS, H., ENGELMAN, R., BEUKES, J.P., VAN ZYL, P.G., RAMANDH, A., NTSANGWANE, L., JOSIPOVIC, M., TIITTA, P., FOURIE, G., NGWANA, I., CHILOANE, K., KOMPPULA, M. 2014. Atmospheric boundary layer top height in South Africa: measurements with lidar and radiosonde compared to three atmospheric models. *Atmospheric Chemistry and Physics*. 14, 4264-4278, doi: 10.5194/acp-14-4263-2014.

KOURTIDIS, K., KELESIS, A., PETRAKAKIS, M. 2007. Hydrogen sulphide (H_2S) in urban ambient air. *Atmospheric Environment*, 42, 7476-7482, doi: https://doi.org/10.1016/j.atmosenv.2008.05.066.

KUIK, F., LAUER, A., BEUKES, J. P., VAN ZYL, P. G., JOSIPOVIC, M., VAKKARI, V., LAAKSO, L., FEIG, G. T. 2015: The anthropogenic contribution to atmospheric black carbon concentrations in southern Africa: a WRF-Chem modeling study, *Atmospheric Chemistry and Physics*, 15, 8809–8830, doi:10.5194/acp-15-8809-2015.

LAAKSO, L., LAAKSO, H., AALTO, P.P., KERONEN, P., PETÄJÄ, T., NIEMINIEN, T., POHJA, T., SIIVOLA, E., KULMALA, M., KGABI, N., MOLEFE, M., MABASO, D., PHALATSE, D., PIENAAR, K. & KERMINEN, V.-M. 2008. Basic characteristics of atmospheric particles, trace gases and meteorology in relatively clean Southern Africa Savannah environment. *Atmospheric Chemistry and Physics*, 8:4823-4839, doi: https://doi.org/10.5194/acp-8-4823-2008.

LAAKSO, L., VAKKARI, V., VIRKKULA, A., LAAKSO, H., BACKMAN, J., KULMALA, M., BEUKES, J.P., VAN ZYL, P.G., TITTA, P., JOSIPOVIC, M., PIENAAR, J.J., CHILOANE, K., GILARDONI, S., VIGNATI, E., WIEDENSOHLER, A., TUCH, T., BIRMILI, W., PIKETH, S., et al. 2012. South African EUCAARI measurements: seasonal variation of trace gases and aerosol optical properties. *Atmospheric Chemistry and Physics*, 12:1847-1864, doi: https://doi.org/10.5194/acp-12-1847-2012.

LAAKSO, L., MERIKANTO, J., VAKKARI, V., LAAKSO, H., KULMALA, M., MOLEFE, M., KGABI, N., MABASO, D., CARSLAW, K. S., SPRACKLEN, D. V., LEE, L. A., REDDINGTON, C. L., KERMINEN, V.-M. 2013. Boundary layer nucleation as a source of new CCN in savannah environment, Atmospheric Chemistry and Physics, 13, 1957–1972, doi:10.5194/acp13-1957-2013.

LABAN, T.L., VAN ZYL, P.G., BEUKES, J.P., VAKKARI, V., JAARS, K., BORDUAS-DEDEKIND, N., JOSIPOVIC, M., THOMPSON, A.M., KULMALA, M., LAAKSO, L. 2018. Seasonal influences on surface ozone variability in continental South Africa and implications for air quality. *Atmospheric Chemistry and Physics,* 18: 15491-15514, doi: https://doi.org/10.5194/acp-18-15491-2018.

LEGAL RESOURCES CENTRE. 2014. Submission on SASOL and Natref's applications for postponement of compliance with the minimum emission standards (MES) under section 21 of the National Environmental Air Quality Act (AQA). https://cer.org.za/wp-content/uploads/2014/06/2014-06-16-LRC-SASOL-NATREF-postponement.pdf. Date of access: [31 May 2019].

LOURENS, A.S.M., BEUKES, J.P., VAN ZYL, P.G., FOURIE, G.D., BURGER, J.W., PIENAAR, J.J., READ, C.E., JORDAAN, J.H. 2011. Spatial and temporal assessment of the gaseous pollutants in the Highveld of South Africa. *South African Journal of Science*, 107(1/2), Art.#297, 8 pages, doi: 10.4102/sajs.v107i1/2.269.

LOURENS, A.S.M., BUTLER, T.M., BEUKES, J.P., VAN ZYL, P.G., BEIRLE, S., WAGNER, T.K., HEUE, K., PIENAAR, J.J., FOURIE, G.D., LAWRENCE, M.G. 2012. Re-evaluating the NO_2 hotspot over the South African Highveld. *South African Journal of Science*, 108(11/12), Art. #1146, 6 pages, doi: http://dx.doi.org/10.4102/sajs.v108i11/12.1146.

LOURENS, A.S.M., BUTLER, T.M., BEUKES, J.P., VAN ZYL, P.G., FOURIE, G.D., LAWRENCE, M.G. 2016, Investigating atmospheric photochemistry in the Johannesburg-Pretoria megacity using a box model, *South African Journal of Science*, 112(1/2), Art. #2015-0169, 11 pages, doi: http://dx.doi.org/10.17159/sajs.2016/2015-0169.

MAENHAUT, W., SALMA, I., CAFMEYER, J., ANNEGARN, H.J., ANDREAE, M.O. 1996. Regional atmospheric aerosol composition and sources in the eastern Transvaal, South Africa, and impact of biomass burning. *Journal of Geophysical Research*, 101:631-650.

MALINOWSKI E.R. 2002. *Factor Analysis in Chemistry*; John Wiley and Sons, Inc.: New York, NY.

MPHEPYA, J. N., PIENAAR, J. J., GALY-LACAUX, C., HELD, G., TURNER, C. R. 2004. Precipitation Chemistry in Semi-Arid Areas of Southern Africa: A Case Study of a Rural and an Industrial Site, *Journal of Atmospheric Chemistry*, 47, 1–24, doi:10.1023/B:JOCH.0000012240.09119.c4.

MPHEPYA, J. N., GALY-LACAUX, C., GALY-LACAUX, J. P., HELD, G., PIENAAR, J. J. 2006. Precipitation Chemistry and Wet Deposition in the Kruger National Park, South Africa, *Journal of Atmospheric Chemistry*, 53, 169–183, doi:10.1007/s10874-005-9005-7.

MUCINA, L., RUTHERFORD, M.C., 2007. The Vegetation of South Africa, Lesotho and Swaziland. SANBI, Pretoria, ISBN: 978-1-919976-21-1.

NKOSI, N.C., PIKETH, S.J., BURGER, R.P. 2018. Fine PM emission factors from residential burning of solid feuls using traditional cast-iron coal stoves. *Clear Air Journal*, 28, doi: http://dx.doi.org/10.17159/2410-972X/2018/v28n1a10.

NOVELLI, P. 2003. Carbon monoxide in the atmosphere. (*In* POTTER, T.D. & COLMAN, B.R., *eds*. *Handbook of weather, climate and water*. Hoboken, N.J.: John Wiley and Sons, Inc. 78-88 p.

PETERSON, J., FISHER, G.W., TIMPANY, G. 1998. Survey of Background Hydrogen Sulphide in Rotorua – 1996/67. AK98013, NIWA.

PETZOLD, A., OGREN, J.A., FIEBIG, M., LAJ, P., LI, S.-M., HOLZER-POPP, T., KINNE, S., PAPPALARDO, G., SUGIMOTO, N., WEHRLI, C., WIEDENSOHLER, A., ZHANG, X.-Y. 2013. Recommendations for reporting "black carbon" measurements. *Atmospheric Chemistry and Physics*, 13, 8365-8379, doi: 10.5194/acp-13-8365-2013.

PIKETH, S.J., VAN NIEROP, M., RAUTNBACH, C., WALTON, N., ROSS, K., HOLMES, S., RICHARDS, T. 2005. Rustenburg Local Municipality Air Quality Management Plan, Palace consulting engineers ltd. Republic of South Africa.

PIRES, J.C.M., SOUSA, S.I.V., PEREIRA, M.C., ALVIM-FERRAZ, M.C.M., MARTINS, F.G. 2007. Management of air quality monitoring using principal component and cluster analysis-Part I: SO_2 and PM10. *Atmospheric Environment*, 42, 1249-1260, doi: 10.1016/j.atmosenv.2007.10.044.

PIRES, J.C.M., SOUSA, S.I.V., PEREIRA, M.C., ALVIM-FERRAZ, M.C.M., MARTINS, F.G. 2008. Management of air quality monitoring using principal component and cluster analysis-Part II: CO, NO_2 and O_3. *Atmospheric Environment*, 42, 1249-1260, doi: 10.1016/j.atmosenv.2007.10.041.

PRETORIUS, I., PIKETH, S.J., BURGER, R., NEOMAGUS, H. 2015. A perspective on South African coal fired power station emissions. *Journal of Energy in Southern Africa*, 26, 27-40.

RAYNER-CANHAM, G., OVERTON, T. 2009. The group 16 elements the chalcogens, in: *Descriptive Inorganic Chemistry*, p 387-388, W.H. Freeman and Compony, New York, NY.

REFF, A., EBERLY, S.I., BHAVE, P.V. 2007. Receptor Modelling of Ambient Particulate Matter Data Using Positive Matrix Factorization: Review of Existing Methods. *Journal of the Air & Waste Management Association*. 57:2, 146-154, doi: 10.1080/10473289.2007.10465319.

REISELL, A., MACDONALD, C., ROBERTS, P., AREY, J. 2003. Characterization of biogenic volatile organic compound and meteorology at Azusa during the SCOS97- NARSTO. *Atmospheric Environment*, 37(Suppl 2):181–196, doi: 10.1016/S1352-2310(03)00390-X.

RIDDLE, E.E., VOSS, P.B., STOHL, A., HOLCOMB, D., MACZKA, D., WASHBURN, K., TALBOT, R.W. 2006, Trajectory model validation using newly developed altitude-controlled balloons during the International Consortium for Atmospheric research and Transport and transformations 2004 campaign. *Journal of Geophysical Research*, 111, D23S57, doi: 10.1029/2006JD007456.

ROSS, K.E., PIKETH, S.J., BRUINTJES, T., BURGER, R.P., SWAP, R.J., ANNEGARN, H.J. 2003. Spatial and seasonal variations in CCN distribution and the aerosol-CCN relationship over southern Africa. *Journal of Geophysical Research*, 108:17-1 - 17-18.

RUBRIGHT, S.L.M., PEARCE, L.L., PETERSON, J. 2017. Environmental toxicology of hydrogen sulfide. *Nitric Oxide*. 71, 1-13, doi: 10.1016/j.niox.2017.09.011.

SAKIRKIN, S.L.P., CASEY, K.D., AUVERMANN, B.W. 2012. Hydrogen Sulfide Emissions from Open/Dry-Lot-Cattle-Feeding Operations. A*ir Quality Education in Animal Agriculture*, http://www.extension.org/pages/15538/air-quality-in-animal-agriculture.

SCHOEMAN, A. 2016. Risk mapping of eMalahleni municipal area with focus on coal mining impacts. Potchefstroom: NWU. (Dissertation – M.Sc.) 134p.

SCOTT, B. 1992. Written communication from Bruce Scott, Bruce Scott, Inc., San Rafael, CA, to David Hendricks, Pacific Environmental Services, Inc., Research Triangle Park, NC, February28.

SEHLOHO, T., BEUKES, J.P., VAN ZYL, P.G., VAKKARI, V., JOSIPOVIC, M., GILARDONI, S., VIGNATI, E., GIANELLE, V., KULMALA, M., LAAKSO, L. 2019. Aerosol composition on the South African Highveld, in preparation for *Atmospheric Environment*.

SEINFELD, J.H., PANDIS, S.N. 2006, Atmospheric Chemistry and Physics: From Air Pollution to Climate Change. Second Edition. P 219. John Wiley & Sons, Inc.

SENGUPTA, A. 2014. Preliminary Hydrogen Sulfide Emission Factors and Emission Models for Wastewater Treatment Plant Headworks. *University of New Orleans Theses and Dissertations*. 1829. https://scholarworks.uno.edu/td/1829.

SHIRAI, H., IKEDA, M., ARAMAKI, H. 2012. Characteristics of hydrogen sulphide formation in pulverized coal combustion*. Fuel*, 114, 114-119, doi: http://dx.doi.org/10.1016/j.fuel.2012.03.028.

SKRTIC, L. 2006. Hydrogen Sulfide, Oil and Gas, and People's Health. Berkeley: University of California. (Dissertation – M.Sc.) 77p.

SLATT, B.J., NATUSCH, D.F.S., PROSPERO, J.M., SAVOIE, D.L. 1967. Hydrogen sulphide in the atmosphere of the northern equatorial Atlantic Ocean and its relation to the global sulfur cycle. *Atmospheric Environment*, 12, 981-991, doi: https://doi.org/10.1016/0004-6981(78)90342-6.

SOUSA, S.I.V., MARTINS, F.G., ALVIM-FERRAZ, M.C.M., PEREIRA, M.C. 2007. Multiple linear regression and artificial neural networks based on principal components to predict ozone concentrations. *Environmental Modelling & Software*, 22, 97–103, doi: 10.1016/j.envsoft.2005.12.002.

STOHL, A. 1998, Computation, accuracy and application of trajectories – a review and bibliography. *Atmospheric Environment*, 32, 947-966, doi: 10.1016/S1352-2310(97)00457-3.

SU, L., YUAN, Z., FUNG, J.C.H., LAU, A.K.H. 2014. A comparison of HYSPLIT backward trajectories generated from two GDAS datasets. *Science of the Total Environment*, 506-507, 527-537, doi: http://dx.doi.org/10.1016/j.scitotenv.2014.11.072.

SUSSMAN, V.H., MULHERN, J.J. 1964, Air Pollution from Coal Refuse Disposal Areas. *Journal of the Air Pollution Control Association*, 14:7, 279-284, doi: 10.1080/00022470.1964.10468282.

SWAP, R. J.; ANNEGARN, H. J.; SUTTLES, J. T.; KING, M. D.; PLATNICK, S.; PRIVETTE, J. L.; SCHOLES, R. J. 2003, Africa burning: A thematic analysis of the Southern African Regional Science Initiative (SAFARI 2000). *Journal of Geophysical Research: Atmospheres***,** *108* (D13), doi: 10.1029/2003JD003747.

THERMO FISHER SCIENTIFIC. 2007. Model 5012 MAAP - Multi Angle Absorption Photometer. Franklin.

THERMO FISHER SCIENTIFIC. 2007. Model 42i – Instruction Manual, Chemiluminescence NO-NO_2_NO_x Analyser. Franklin.

TIITTA, P., VAKKARI, V., CROTEAU, P., BEUKES, J.P., VAN ZYL, P.G., JOSIPOVIC, M., VENTER, A.D., JAARS, K., PIENAAR, J.J., NG, N.L., CANAGARATNA, M.R., JAYNE, J.T., KERMINEN, V.-M. KOKKOLA, H., KULMALA, M., LAAKSONEN, A., WORSNOP D.R. AND LAAKSO, L. 2014. Chemical composition, main sources and temporal variability of PM1 aerosols in southern African grassland, *Atmospheric Chemistry and Physics*, 14, 1909–1927, doi:10.5194/acp-14-1909-2014.

TUMMON, F., SOLMON, F., LIOUSSE, C., TADROSS, M. 2010. Simulation of the direct and semidirect aerosol effects on the southern Africa regional climate during the biomass burning season, *Journal of Geophysical Researsch*, 115, D19206, doi:10.1029/2009JD013738.

TYSON, P.D., D'ABRETON, P.C. 1998. Transport and recirculation of aerosols off Southern Africa – macroscale plume structure. *Atmospheric Environment*, 32, 1511-1524, doi: https://doi.org/10.1016/S1352-2310(97)00392-0.

VAN DER MERWE, C., SUKDEO, P., PETA, S., SMIT, D. 2017. Eskom Low NOx burner combustion simulation experience*. 2017 ANSYS Engineering Simulation Conference*. https://www.researchgate.net/publication/329443440_ESKOM_Low_NOx_burner_combustion_simulation_experience_-_A_Low_NOx_burner_design_case_study.

VAN ZYL, P.G., BEUKES, J.P., DU TOIT, G., MABASO, D., HENDRIKS, J., VAKKARI, V., TIITTA, P., PIENAAR, J.J., KULMALA, M. AND LAAKSO, L. 2014. Assessment of atmospheric trace metals in the western Bushveld Igneous Complex, South Africa, *South African Journal of Science*, 110(3/4), Art. #2013-0280, 11 pages, doi: https://doi.org/10.1590/sajs.2014/20130280.

VAKKARI, V., LAAKSO, H., KULMALA, M., LAAKSONEN, A., MABASO, D., MOLEFE, N., LAAKSO, L. 2011. New particle formation events in semi-clean South African savannah. *Atmospheric Chemistry Physics*, 11:3333-3346.

VENTER, A.D., VAKKARI, V., BEUKES, J.P., VAN ZYL, P.G., LAAKSO, H., MABASO, D., TIITTA, P., JOSIPOVIC, M., KULMALA, M., PIENAAR, J.J. & LAAKSO, L. 2012. An air quality assessment in the industrialised western Bushveld Igneous Complex, South Africa. *South Africa Journal of Science*, 108:1-10, doi: http://dx.doi.org/10.4102/sajs.v108i9/10.1059.

VENTER, A.D., VAN ZYL, P.G., BEUKES, J.P., JOSIPOVIC, M., HENDRIKS, J., VAKKARI, V., LAAKSO, L. 2017. Atmospheric trace metals measured at a regional background site (Welgegund) in South Africa, *Atmospheric Chemistry and Physics*, 17, 4251–4263, doi:10.5194/acp-17-4251-2017.

VENTER, M., BEUKES, J.P., VAN ZYL, P.G., VAKKARI, V., VIRKKULA, A., JOSIPOVIC, M., KULMALA, M., LAAKSO, L. 2019. Long-term observations of aerosol optical properties at a southern African grassland savannah site, in preparation for *Atmospheric Chemistry and Physics*.

VIANA, M., KUHLBUSCH, T.A.J., QUEROL, X., ALASTUEY, A., HARRISON, R.M., HOPKE, P.K., WINIWARTER, W., VALLIUS, M., SZIDAT, S., PRÉVÔT, A.S.H., HUEGLIN, C., BLOEMEN, H., WÅHLIN, P., VECCHI, R., MIRANDA, A.I., KASPER-GIEBL, A., MAENHAUT, W., HITZENBERGER, R. 2008. Source apportionment of particulate matter in Europe: A review of methods and results. *Journol of Aerosol Science,* 39, 827-849, doi: 10/1016/j.jaerosci.2008.05.007.

VISSER, H., BURING, E., BREUGEL, P.B. 2001. Composition and origin of airborne particulate matter in the Netherlands. *National Institute for Public Health and the Environment*, RIVM.

WAGMULLER, M., PETERSON, J. 1998. Method to quantify the H_2S – Exposure for the urban area of Rotorua. AK98024, NIWA.

WANG, S., XIAO, F. 2004. AHU sensor fault diagnosis using principal component analysis method. *Energy and Buildings*, 36 (2), 147–160, doi: 10.1016/j.enbuild.2003.10.002.

WELLS, R., LLOYD, S., TURNER, C. 1996. National air pollution source inventory, in: Air pollution and its impacts on the South African highveld, (Eds) Held, G., Gore, B. J., Surridge, A. D., Tosen, G. R., Turner, C. R., and Walmsley, R. D., 3–9, *Environmental Scientific Association*, Cleveland.

WENIG, M., SPICHTINGER, N., STOHL, A., HELD, G., BEIRLE, S., WAGNER, T., JÄHNE, B., PLATT, U. 2003. Intercontinental transport of nitrogen oxide pollution plumes. *Atmospheric Chemistry and Physics*, 3, 387-393, doi: https://doi.org/10.5194/acp-3-387-2003.

WILLIAMS, P.I., BALTENSPERGER, U. 2009. Particulate matter in the atmosphere. (*In* HEWITT, C.N. & JACKSON, A.V., *eds. Atmospheric Science for Environmental Scientists*. Chichester, W. Sussex: Wiley-Blackwell. 168-197 p.)

WOLD, S., ESBENSEN, K., GELADI, P. 1987. Principal component analysis. *Chemometrics and Intelligent Laboratory Systems*. 2, 1-3, 37-52, doi: 10.1016/0169-7439(87)80084-9.

WORLD HEALTH ORGANIZATION. 2003. Hydrogen Sulphide: Human health aspects. *Concise international chemical assessment document*; 53. ISBN: 92 4 1530537, ISSN: 1020-6167.

XIAO, Z., LAPLANTE, A.R. 2004. Characterizing and recovering the platinum group minerals-a review. *Mnerals and Engineering*, 17, 961-979 doi: 10.1016/j.mineng.2004.04.001.

YARWOOD, G., MORRIS, R.E., WILSON, G.M. 2007. Particulate Matter Source Apportionment Technology (PSAT) in the CAMx Photochemical Grid Model. *Air Pollution Modeling and its Application XVII.* Springer, Boston, MA, doi: https://doi.org/10.1007/978-0-387-68854-1_52.

ZUNCKEL, M., TURNER, C.R., WELLS, R.B., 1996. Dry deposition of sulphur on the Mpumalanga highveld: a pilot study using the inferential method. *South African Journal of Science*, 92 (10), 485-491, doi: http://hdl.handle.net/10204/719.

ZUNCKEL, M., ROBERTSON, L., TYSON, P.D., RODHE, H., 2000. Modelled transport and deposition of sulphur over Southern Africa. *Atmospheric Environment*. 34, 2797-2808, doi: 10.1016/S1352-2310(99)00495-1.

Appendix A

Table 4.3: Table of statistical values from the box plot in Figure 4.1.

	2009											
		Feb	**Mar**	**Apr**	**May**	**Jun**	**Jul**	**Aug**	**Sep**	**Oct**	**Nov**	**Des**	
Min		-0.7	-0.8	-0.3	-0.4	-0.1	-0.6	-0.1	-0.5	-0.3	-0.3	-0.8	
Max		36.4	29.8	49.2	57.2	119.3	62.3	55.0	63.7	25.5	24.7	58.0	
Mean		2.1	2.3	3.7	3.2	5.3	5.3	3.4	3.4	2.1	2.1	3.4	
Median		1.4	1.8	2.2	1.6	3.9	2.8	1.9	1.8	1.5	1.4	2.3	
5th Percentile		0.3	0.4	0.8	0.3	0.7	0.6	0.4	0.4	0.3	0.3	0.7	
25th Percentile		0.9	1.3	1.5	0.9	1.9	1.6	1.3	1.1	0.9	0.8	1.5	
75th Percentile		2.2	2.4	3.6	3.5	5.4	5.7	3.4	3.7	2.2	2.5	3.2	
95th Percentile		6.8	6.3	12.7	12.2	16.4	20.7	11.2	12.4	6.6	7.0	10.3	
	2010												2011
	Jan	**Feb**	**Mar**	**Apr**	**May**	**Jun**	**Jul**	**Aug**	**Sep**	**Oct**	**Nov**	**Des**	**Jan**
Min	-1.7	-0.1	-0.3	-0.4	-1.3	-0.5	0	-0.3	-1.3	-0.8	-0,8	-0.2	-0.4
Max	29.2	38.3	43.8	28.1	61.3	86.1	40.6	56.1	39.3	60.4	62.1	92.0	32.6
Mean	2.6	2.7	2.3	2.5	3.1	4.9	2.7	3.0	3.9	2.6	2.6	2.5	1.4
Median	1.9	1.7	1.2	1.5	1.8	2.2	1.5	1.5	2.2	1.8	1.5	1.4	0.9
5th Percentile	0.5	0.4	0.4	0.5	0.2	0.8	0.3	0.3	0.3	0.3	0.3	0.3	0.2
25th Percentile	1.5	1.1	0.9	1.0	1.1	1.5	0.8	1.0	1.4	1.0	0.9	0.8	0.6
75th Percentile	2.8	2.6	1.9	2.5	2.7	4.7	2.3	3.0	4.2	3.1	2.6	2.3	1.3
95th Percentile	6.5	8.6	8.4	8.7	11.4	18.0	11.2	10.9	14.0	8.0	9.2	9.7	3.9